



Theses and Dissertations

2007-03-20

An Investigation of Wear-Resistant Coatings on an A390 Die-Cast Aluminum Substrate

D. Adam Mower
Brigham Young University - Provo

Follow this and additional works at: <https://scholarsarchive.byu.edu/etd>



Part of the [Mechanical Engineering Commons](#)

BYU ScholarsArchive Citation

Mower, D. Adam, "An Investigation of Wear-Resistant Coatings on an A390 Die-Cast Aluminum Substrate" (2007). *Theses and Dissertations*. 851.

<https://scholarsarchive.byu.edu/etd/851>

This Thesis is brought to you for free and open access by BYU ScholarsArchive. It has been accepted for inclusion in Theses and Dissertations by an authorized administrator of BYU ScholarsArchive. For more information, please contact scholarsarchive@byu.edu, ellen_amatangelo@byu.edu.

AN INVESTIGATION OF WEAR-RESISTANT COATINGS
ON AN A390 DIE-CAST ALUMINUM SUBSTRATE

by

David A. Mower

A thesis submitted to the faculty of

Brigham Young University

in partial fulfillment of the requirements for the degree of

Master of Science

Department of Mechanical Engineering

Brigham Young University

April 2007

BRIGHAM YOUNG UNIVERSITY

GRADUATE COMMITTEE APPROVAL

of a thesis submitted by

David A. Mower

This thesis has been read by each member of the following graduate committee and by majority vote has been found to be satisfactory.

Date

Robert H. Todd, Chair

Date

Spencer P. Magleby

Date

Carl D. Sorensen

BRIGHAM YOUNG UNIVERSITY

As chair of the candidate's graduate committee, I have read the thesis of David A. Mower in its final form and have found that (1) its format, citations, and bibliographical style are consistent and acceptable and fulfill university and department style requirements; (2) its illustrative materials including figures, tables, and charts are in place; and (3) the final manuscript is satisfactory to the graduate committee and is ready for submission to the university library.

Date

Robert H. Todd
Chair, Graduate Committee

Accepted for the Department

Matthew R. Jones
Graduate Coordinator

Accepted for the College

Alan R. Parkinson
Dean, Ira A. Fulton College of Engineering
and Technology

ABSTRACT

AN INVESTIGATION OF WEAR-RESISTANT COATINGS ON A390 DIE-CAST ALUMINUM SUBSTRATE

David A. Mower

Department of Mechanical Engineering

Master of Science

In this investigation, four coatings were tested for their ability to increase the wear life of A390 aluminum primary clutch sheaves used in continuously variable transmission (CVT). The coatings tested were: hard chrome, electroless nickel metal, hard coat anodizing and composite ceramic coating. The primary clutch sheave material is a die-cast A390 aluminum.

A wear test stand was developed to duplicate wear found on CVTs currently in use. The wear was evaluated using four methods. First, the change in shift characteristics of the CVT while running on the wear test stand, second a change in performance using an ATV and chassis dynamometer, third the amount of material lost, through wear, was measured using a profilometer, and finally a scanning electron microscope which was used to identify the dominate mechanism of wear in the sheave material.

All of the tests showed the hard chrome coating to have the lowest wear rates and the best wear characteristics. The electroless nickel metal coating did improve the wear life of the CVT but had very high variation. The hard coat anodized and ceramic composite coatings were eliminated early in testing because of poor performance.

ACKNOWLEDGMENTS

I would like to acknowledge Dr. Robert H. Todd my advisor for his continual patience, encouragement, and guidance, also my committee members Dr. Spenser Magleby and Dr. Carl Sorensen for their great support.

I would also like to thank Polaris Industries, Inc. namely Jeff Bennett and Steve Nelson for making this research possible.

I would like to give a special thanks to Kevin Cole for his great help. Thanks to my family and all the many others who supported and encouraged me in this research.

TABLE OF CONTENTS

1	Introduction.....	1
1.1	Continuously Variable Transmissions	1
1.2	Discussion of Wear	4
1.3	Problem Statement and Objectives	5
1.4	Benefits of a Solution	6
1.5	Overview of Thesis	6
2	Wear Theory Related to the CVT	7
2.1	Wear in a CVT	8
2.2	Dry Sliding Wear	9
2.3	Repeated Cycle Deformation.....	17
2.4	Wear Behavior of Aluminum and Coated Aluminum	23
2.5	Wear hypothesis.....	27
3	Methods and Procedures	29
3.1	Proposed solutions to the wear problem	30
3.2	Test procedures	35
3.3	Determining dominant wear mechanism	49
3.4	Summary of Testing and Methods.....	50
4	Results	51

4.1	Wear Test Stand Results	52
4.2	Dynamometer Results	57
4.3	Profilometer Results	62
4.4	Scanning Electron Microscope Results	67
4.5	Summary of Results	75
5	Conclusions and Future Work.....	77
5.1	Recommendations.....	77
5.2	Future Work.....	78
	References.....	79
	Appendix A – Hydraulic Fluid Specifications	81
	Appendix B – Labview Block Diagram.....	83
5.3	Clutch_Testing_Program.vi	83
5.4	Acquire_Data.vi.....	84
5.5	Control.vi	84
5.6	Motor_On_Time.vi	85
	Appendix C – Hommel Tester T8000 Specifications	87
	Appendix D – Clutch Run Order	89
	Appendix E – MATLAB 7.0 m-file code.....	91
	Appendix F – Shift delay plots.....	93
	Appendix G – ANOVA and MATLAB 7.0 code	97

Appendix H – Wear Profiles	101
Appendix I – Statistics for shift delay	95
Appendix J – Plots for comparing shift delay	113

LIST OF TABLES

Table 3-1 Tested coatings and their coating process	31
Table 3-2 First stage test values.....	38
Table 4-1 Change in slope data for Acceleration and Backshift	60
Table 4-2 Summary of ANOVA results	61
Table 4-3 Summary of contrasts.....	62
Table 4-4 Average surface roughness of new clutches.....	65
Table 4-5 Average of surface roughness measurements taken after 25 hours of testing.....	66
Table 4-6 Comparison of adhesive wear to uncoated clutches.....	69
Table 4-7 Wear characteristics compared to fatigue wear.....	72
Table 4-8 adhesive wear compared with hard chrome.....	75

LIST OF FIGURES

Figure 1-1 CVT complete assembly.	2
Figure 1-2 Primary Clutch: 1) moveable sheave, 2) fixed sheave, 3) spring, 4) weights, 5) spider.	2
Figure 2-1 Examples of wear scar morphology on metal surfaces, resulting from single-cycle deformation during sliding contact. A-D, F, and G are from three-body abrasive wear situations. E is a wear scar resulting from a single sliding stroke between a hard ball and a softer flat [3].	11
Figure 2-2 Picture A shows adhesive wear or galling at a normal pressure above the threshold pressure. Picture B shows adhesive wear below the threshold pressure [3].	13
Figure 2-3 Examples of wear scars, in varying degrees, resulting from three-body abrasion [3].	16
Figure 2-4 Examples of the influence of the nature of stress system on crack formation [3].	19
Figure 2-5 General nature of the stress field in contact situation, illustrating the relative effects of contact geometry and asperities on stress[3].	20
Figure 2-6 Wear scar morphology of single-crystal copper in lubricated sliding [3].	22
Figure 2-7 A - C Shows the progression of severe rolling contact wear. C shows normal rolling contact fatigue wear scar [3].	22
Figure 2-8 (Previous Page): 1) Cross section of a 2014-T6 sheave wheel specimen indicating adhesive and abrasive wear 2) Wear Surface of 2014-T6 sheave wheel specimen indicating abrasive wear (grooves) and wear particles at B 3) Cross section of a 2014-T6 specimen indicating adhesive wear (lines of shear induced plastic deformation) 4) Cross section of a 2014-T6 specimen revealing aluminum-oxide particle formation at D 5) Wear surface of a 2014-T6 specimen indicating adhesive wear (galling) and abrasive wear (grooves at C) 6) Cross-section of 7050-T7451 specimen indicating adhesive wear (lines of shear-induced plastic deformation with void formation and coalescence at E) [10].	24

Figure 3-1 First stage test stand.	37
Figure 3-2 Second stage wear test stand.	39
Figure 3-3 Labview front panel for second stage test stand.	41
Figure 3-4 Labeled primary clutch.	43
Figure 3-5 Hommel Layout	44
Figure 3-6 Start point for stylus	46
Figure 3-7 Example acceleration plot.	47
Figure 3-8 Dynamometer testing	48
Figure 4-1 Example plot taken from B-2. The blue line is pressure in psi the green line is rpm of the secondary clutch.	53
Figure 4-2 Average shift delay of tested primary clutches.	54
Figure 4-3 Hard chrome shift delay with first 25 hours of A2 test.	55
Figure 4-4 Belt width measurements after 25 hours of testing	57
Figure 4-5 Example of formatted acceleration curves.	58
Figure 4-6 Example of acceleration slope.	59
Figure 4-7 Plots showing the change in slope with wear.	60
Figure 4-8 Profilometer profile of a moveable sheave after 25 hours of wear.	63
Figure 4-9 Plot showing cross sectional area of wear groove.	64
Figure 4-10 Example profile of the two groove trend; where A is the shallow groove, B is the peak, and C is the deep groove.	65
Figure 4-11 Large area view uncoated wear surface A) Large Si grain B) Radial abrasive scar. Radial direction is vertical.	67
Figure 4-12 Silicon grain with brittle fracture A) Striations in the Si grains, B) Radial wear scar. Radial direction is vertical.	68
Figure 4-13 Large silicon grain, radial direction is vertical.	68
Figure 4-14 Example of surface fatigue. Radial direction is vertical.	70

Figure 4-15 Example of abrasion A) radial abrasive wear scars. Radial direction is vertical.....	71
Figure 4-16 Possible delimitation. Radial direction is vertical.....	72
Figure 4-17 Area of high wear A) worn area B) Rough low area C) pits in coating. Radial direction is horizontal.....	73
Figure 4-18 No visible abrasive or surface fatigue wear scars. Radial direction is horizontal.	74
Figure 4-19 Large particle lost due to surface defect. Radial direction is horizontal.....	74

1 Introduction

Since the first mechanical devices were used in daily life, wear, in all of its forms, has been a problem for engineers. As mechanical devices have improved and become higher performing, wear has become an increasingly difficult problem to solve. Larger forces, higher temperatures, faster speeds, and harsher environments are all contributors to the problem of wear. Even in applications where a relatively soft object is coming in contact with a hard surface, the hard surface will wear. Such is the case with a Continuously Variable Transmission (CVT), where a V-belt will wear grooves in the aluminum sheaves of a CVT. The objective of this chapter is to briefly describe the CVT, the wear that may be present in CVT sheaves, and the problems that the wear causes.

1.1 Continuously Variable Transmissions

Continuously Variable Transmissions are used on all-terrain vehicles (ATV) and snowmobiles. The CVT is an automatic transmission and clutch (this is why components of the CVT are often referred to as clutches). The CVT is a belt and pulley system that uses a V-belt to transfer power from a primary or drive clutch to a secondary or driven clutch, see Figure 1-1. The belt is a composite made of Neoprene rubber that is loaded with Aramid fiber and has an Aramid cord as the tensile member.

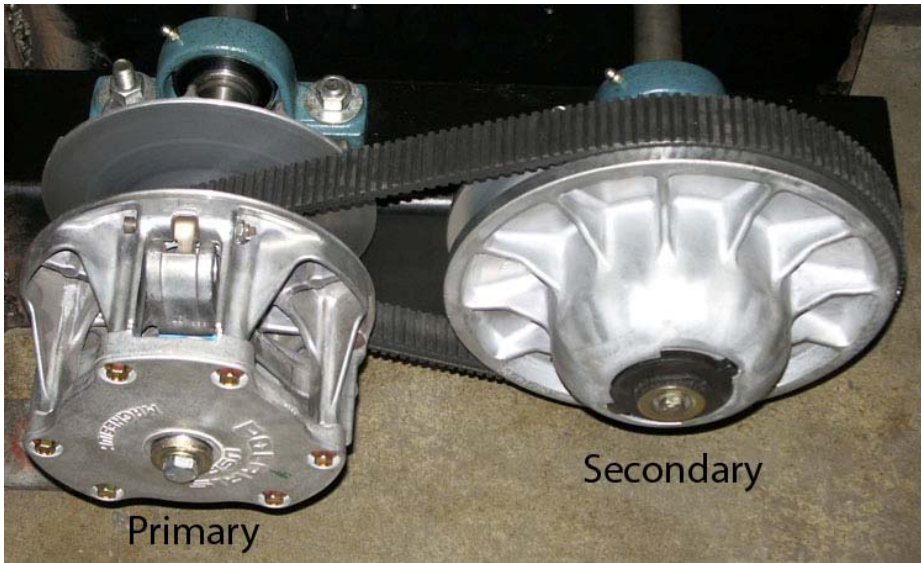


Figure 1-1 CVT complete assembly.



Figure 1-2 Primary Clutch: 1) moveable sheave, 2) fixed sheave, 3) spring, 4) weights, 5) spider.

The primary clutch is composed of fixed and movable sheaves, a spring, weights and spider (see Figure 1-2). The primary clutch is fixed to the end of the crankshaft on the outside of the crankcase. As the engine rpm increases, the centripetal force of the weights in the drive clutch push against the spider, producing a clamping force on the belt between the sheaves. Thus, the engagement of the drive clutch is directly related to the rpm of the engine. Because of this, the CVT acts as a clutch and a variable transmission. When the primary clutch is spinning at a relatively low rpm, the clamping force is low and allows the belt to slip, acting as a clutch. As the drive clutch's rotational speed increases, the clamping force fully engages the CVT and forces the belt to a larger radius on the sheave, effectively changing the CVT to a higher gear. The secondary or driven clutch, uses a torsional spring and helix cam to make the CVT sensitive to torque. A high torque load causes a higher clamping force in the secondary clutch. If the torque load is low and the engine rpm is high, the primary clutch will be able to overcome the force of the torsion spring in the secondary clutch and shift into a higher gear. As the torque load is increased, the engine speed slows and the clamping force in the primary clutch is reduced. The clamping force produced by the torsion spring and helix in the secondary clutch will then increase, forcing the CVT into a lower gear.

Because of the many weights and springs that can be used and other factors involved, such as belt slippage and varying radii of the belt position, the CVT it is a very difficult mechanism to model. This has caused the development of the CVT to be somewhat of a black art, using the evolutionary search method to explore the design space. The lack of a model also makes improving the CVT difficult, because it is difficult to predict the behavior of the CVT in certain loading conditions. For example,

as a CVT is used the belt will wear grooves into the sheaves of the primary clutch causing a change in performance. To solve this wear problem, extra experimentation is required to develop a test cycle so the mechanism of wear can be tested. From the information learned in this experimentation, a test stand could be built to reproduce the wear grooves found in the primary clutch. Optimizing the test stand for maximum wear rates without deviating from real-world wear situations is also a challenge.

1.2 Discussion of Wear

As with many engineering problems, there is no closed form governing model for wear. This is due in part to the many factors of wear and the many mechanisms that cause wear. Many experiments have been accomplished to analyze the effects of different factors in the various mechanisms of wear. The majority of these experiments have been for metal to metal contact. There is very little to be found in the literature on the wear of a coated material and even less to be found concerning the wear of a metal caused by a nonmetal. Chapter 2 discusses wear theories and mechanisms of wear as they might apply to the CVT.

The most relevant literature on wear of the CVT is Michael Whiting's masters thesis, in which he researched the effects of surface hardness on wear resistance [1]. Michael Whiting used a modified Tabor test to analyze the effects of hard coat anodized CVT sheaves on the wear resistance of the sheaves. His conclusions indicated that hardness does affect wear resistance; however, hardness is not the only factor. Surface finish can also be a major contributor. Whiting's research found that although hard-coat anodized A390 die-cast aluminum had a much harder surface than normal A390

aluminum, it did not wear as long as predicted. It was concluded that this was due in part to its very porous surface finish. Other texts state that (in addition to hardness and surface roughness) load, speed, environment, and temperature also affect wear rates [1, 2].

For the wear application of the CVT, the principle parameters that can be varied include surface hardness, surface roughness, and the integrity and bond strength of the coating to the aluminum substrate.

1.3 Problem Statement and Objectives

Under a number of situations in which an ATV may be used, the composite V-belt develops premature wear grooves in the sheaves of the primary clutch. These grooves typically develop in the low gear range of the CVT. This wear causes a significant drop in the performance of the vehicle. As the ATV accelerates, the belt essentially becomes stuck in the grooves, requiring more engine rpm to move the belt out of the groove. When the belt comes out of the groove, it causes the vehicle to lurch. In many cases this wear is premature, developing in as little as 1,000 miles, and falls under the coverage of the vehicle warranty. Evidence from a preliminary investigation indicates that the riding conditions that cause this premature wear are riding at low speeds with high loads, such as using a pull-behind lawn mower. Although the conditions under which the premature wear is taking place are known, the mechanism of wear, or the manner in which material is removed from the face of the clutch sheaves, is not well understood.

The primary objective of this research was to gain additional knowledge of this wear phenomenon and learn how to mitigate it so that cost effective design changes could be made to CVT sheaves that will result in longer-wearing CVT clutches. In order to accomplish this objective, experimentation was devised to determine the wear rates of stock clutch sheaves as well as coated sheaves intended to improve wear resistance. The main mechanism of wear was determined by observing wear scars and wear conditions.

1.4 Benefits of a Solution

Understanding the surface interactions in which the wear is caused, that is, a composite polymer and elastomer on aluminum in rolling and sliding contact forces would enable the designer to better choose methods to counter the effects of wear. Understanding how coatings affect wear rates in this mechanism of wear will help designers and coaters choose and design more appropriate coatings for wear resistance.

For the CVT, understanding the wear mechanism and solving the wear problem will not only save money but improve the performance of CVTs.

1.5 Overview of Thesis

As previously stated, chapter 2 discusses the wear theory and mechanisms of wear that are believed to be relevant to a CVT. Chapter 3 discusses the test procedure used and the methodology for classifying wear mechanisms based on micrographs of wear surfaces. Chapter 4 contains the results of the performance and measurement tests as well as the dominant wear classification. Chapter 5 discusses these results and their inferences and gives recommendations for future work.

2 Wear Theory Related to the CVT

Nearly every mechanism will experience some form of wear throughout its time in service. For every different set of operating conditions, different factors can contribute to the wear of mechanical components. Typically, sliding is the most common factor identified as the cause of wear. However, many parts will experience wear from other surface interfaces and environment interactions. Temperature change, oxidation, corrosion, tribofilm, abrasives, and impact loading can all contribute to the mechanism of wear [3]. In fact, these mechanisms of wear often have subcategories further detailing how and why wear is occurring. This chapter will give a brief overview of the general wear theory. Because there is such a large amount of information on all of the different wear types, this chapter will discuss only those types wear that are believed to be related to a belt and pulley system such as a CVT namely adhesive wear, abrasive wear, and repeated-cycle deformation wear or surface fatigue wear. This chapter will also discuss current research that is related to the wear of aluminum. No research was found on the wear behavior of a nonmetal wearing a metal.

Models for wear mechanisms are usually empirically based or have empirically found coefficients. This makes the equations somewhat unreliable and difficult to use in areas that have not been tested. It also makes identifying the mechanism of wear very important. The most commonly used method of identifying wear mechanisms is by

studying the wear surface characteristics of worn materials. Depending on the wear mechanism, these characteristics may be seen with the naked eye, or may require a Scanning Electron Microscope (SEM).

2.1 Wear in a CVT

As with most mechanical devices, many different mechanisms of wear take place at the same time in a CVT. Typically there is one mechanism of wear that is the primary cause of the wear and failure of the device; this mechanism is usually called the dominant wear mechanism [3]. By examining how the belt and the sheaves of the primary clutch contact each other it will show the possible modes of wear.

Because the CVT acts as a clutch and is unlubricated, dry sliding wear occurs. With dry sliding wear comes the possibility of single-cycle deformation and/or repeated-cycle deformation. Repeated-cycle deformation in dry sliding wear will usually show up in the form of adhesive wear. Single-cycle deformation will typically show up as an abrasive wear where particles will scar the face of the clutch in one pass. When the CVT is acting as a transmission, the primary clutch will go through many thousands of loading cycles in a minute. The sheaves experience a normal load and shear load. The normal loading is similar to needle bearing load. The main cause of wear in a bearing load is surface fatigue.

Thermal, oxidative, and corrosive wear may be present, but it is highly unlikely that they are the primary mechanism of wear, because the temperature changes are relatively small, the sheaves are not given time to oxidize between cycles, and the environment is not corrosive.

2.2 Dry Sliding Wear

Dry sliding wear is a very broad category of wear, and subcategories are often used to further define the mechanism of wear. This section will discuss in detail the subcategories of dry sliding wear that are found in the CVT.

2.2.1 Single-Cycle Deformation

Single-cycle deformation wear often occurs under dry sliding conditions and is caused by a hard material producing plastic deformation, permanent displacement, or removal of material in a single engagement [3]. The deformation occurs when an asperity of a hard material plows, wedge-forms, cuts, or micro-cracks the surface of softer material. Although there is deformation with every engagement, the amount of material removed can be very small and can take many cycles to become apparent. However, in most cases this type of wear is the most severe and has the highest wear rates.

The governing equation of single-cycle deformation is:

$$V = \frac{KPx}{p} \quad (2.1)$$

where V is the total volume lost, P is the normal force pressing the two surfaces together, x is the sliding distance, and p is the penetration hardness of the softer material. The constant K is dependent on the materials and the mode of wear. It is important to note that the value of K will change with each different wear situation. The units of this and all other wear models shown in chapter 2 will be dependent and must remain consistent with the units of the experimentally found value for K . The model also assumes that the

asperities are conical shapes on the hard surface and that the softer surface is relatively smooth [3].

Single-cycle deformation can be its own mode of wear, or it can be categorized with other types of wear such as abrasive or adhesive wear in the case that it meets the basic definition of single-cycle deformation.

Wear scars that result from single-cycle deformation can sometimes be visible with the naked eye. These scars will be striations in the direction of motion and are often shinier than the unworn material because they have not yet had time to oxidize. Sometimes a microscope is needed to see the deformation. Figure 2-1 shows examples of the different modes of single-cycle wear.

2.2.2 Adhesive Wear

Adhesive wear is another type of wear that occurs under dry sliding conditions. Adhesive wear follows the theory that a surface is not perfectly smooth but consists of many small asperities that create varying degrees of roughness. Since each of the two mating surfaces is made up of these asperities, the real contact area is not the total surface area of the two mating surfaces or the apparent contact area. As the normal force between two surfaces increases, the number and degree of asperities contacting each other increases. When a shear stress is applied to the contacting asperities, plastic or elastic deformation can occur. The amount of plastic or elastic deformation that will occur depends on many factors, including surface roughness and normal force. The surface roughness and the normal force determine the ratio between the real contact and the apparent contact area. Junction size, frequency, and the plasticity index will also play roles in the amount of plastic and elastic deformation [4].

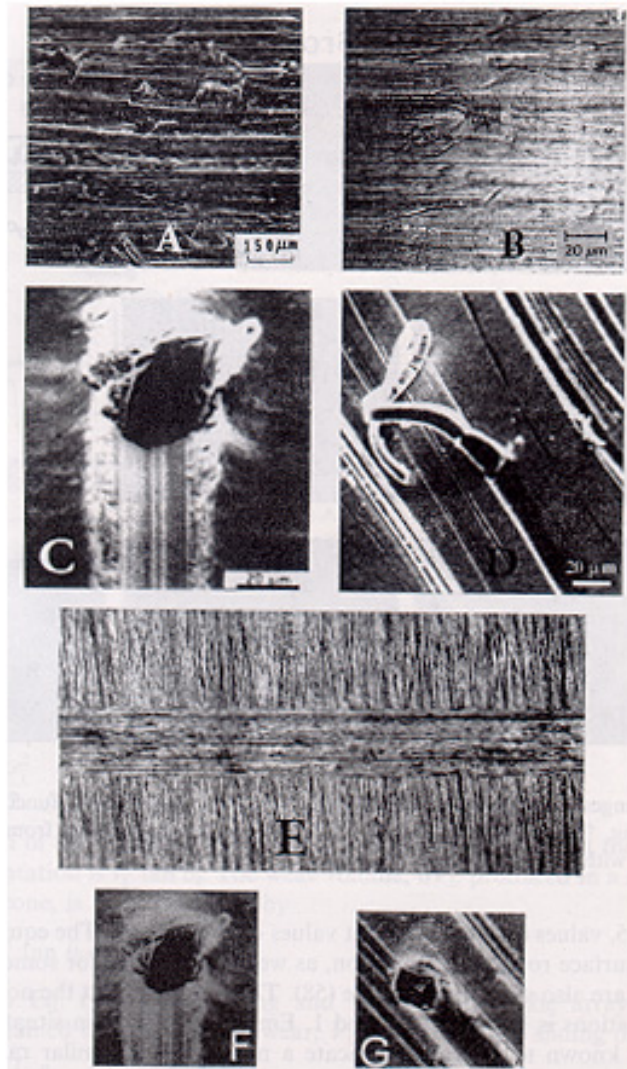


Figure 2-1 Examples of wear scar morphology on metal surfaces, resulting from single-cycle deformation during sliding contact. A-D, F, and G are from three-body abrasive wear situations. E is a wear scar resulting from a single sliding stroke between a hard ball and a softer flat [3].

Adhesive wear must be considered on the atomic level as well as the asperity level. Atomic forces are very weak when the distance between the atoms is relatively large. As the distance becomes relatively close, the attractive forces become very strong and as the atoms get closer still, the forces become repulsive. When asperities come in

contact with each other, the distances between atoms of the two surfaces are such that bonding can occur. Because the two mating surfaces do not have to be sliding relative to each other for this proximity to occur, bonds can be formed in an impact or bearing loading condition. As the surfaces move relative to each other, these bonds are broken and material loss may result [4].

Modeling this behavior was first done empirically by Archard, and Archard makes some key assumptions about the surfaces which are in contact with each other [5]. The Archard equation (see equation (2.2)) assumes that the real contact areas are circles, the asperities are hemispheres, and that the worn material has a lower tensile strength than the wearing material.

$$V = \frac{K}{3p} Px \quad (2.2)$$

For Archard's equation above, V is the total volume loss, K is the probability that a given bond will be strong enough to remove the material from the asperity, p is penetration hardness of the softer material, P is the normal force of the two contacting surfaces, and x is the sliding distance. The K probability takes into account such factors as surface roughness and whether or not there are contaminants or lubrication between the sliding surfaces [5].

Galling is a severe form of adhesive wear that occurs when the contact pressure is above a threshold stress and causes more severe wear [6]. Galling will yield highly deformed protrusions and plastic deformation. Figure 2-2 shows examples of adhesive wear surfaces.

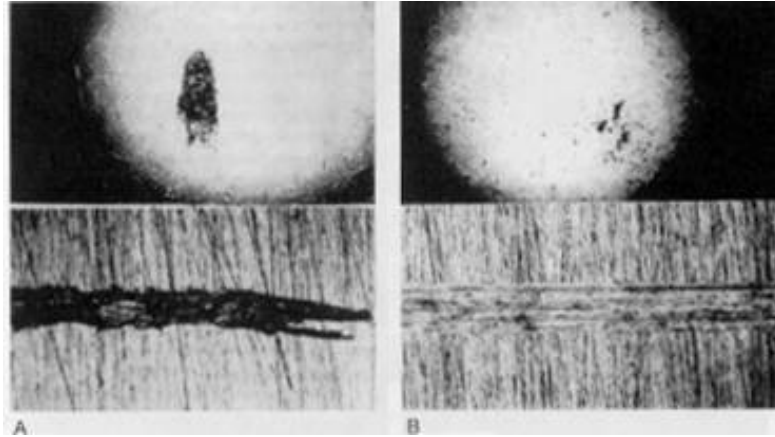


Figure 2-2 Picture A shows adhesive wear or galling at a normal pressure above the threshold pressure. Picture B shows adhesive wear below the threshold pressure [3].

Figure 2-2 shows material being removed by the round pins, (the upper pictures), from the wear surfaces, (the lower pictures). The dark area on the pins is the material from the wear surface. Picture A, showing galling, has much more material loss than picture B, showing normal adhesion wear, because the normal force is higher than the threshold pressure.

Although the belt components may not bond to aluminum in the same way metal bonds to another metal, it is still possible for adhesive wear to take place. This follows that dissimilar metals have lower adhesion wear rates [4]. In most cases, because rubber has a lower tensile strength than aluminum, it is less likely that adhesive wear is taking place in this CVT example. However, it is possible that the rubber may remove asperities from the aluminum if the rubber asperity is much larger than the aluminum asperity. A very large rubber asperity would essentially envelop a small aluminum asperity, giving it a large enough cross section to remove the smaller asperity. Although the tensile strength of Aramid fibers is much higher than that of aluminum, and the Aramid fibers are often

exposed to the aluminum, the likelihood that it is causing adhesive wear is small because it is unlikely that the Aramid is bonding to the aluminum. Also, since the Aramid is made up of woven fibers, it is not likely that there are typical asperities coming in contact with the aluminum surface.

Because the interaction between the aluminum and the Neoprene and Aramid fibers is not fully understood, it can be seen that Archard's equation and the assumptions that are made in using the equation would not apply directly to the CVT wear situation.

2.2.3 Abrasive Wear

Abrasive wear is typically broken up into two types, two-body abrasion and three-body abrasion. Erosion is sometimes labeled as a category of abrasive wear in cases where there is only one surface and free abrasive particles. However, erosion is not present in a CVT; therefore, it will not be discussed in detail. Extreme examples of two body abrasion are grinding or sanding. Three body abrasion would be sand in a bearing or metal particles in a transmission. In both cases, abrasive wear can be single-cycle deformation or repeated-cycle deformation depending on material hardness [7]. In the CVT, because the belt is much softer than the aluminum sheaves, single-cycle deformation is unlikely, making the two-body abrasion most likely due to repeated-cycle deformation. However, three-body abrasion caused by single-cycle deformation is likely to be taking place, because foreign particles, such as dirt, sand, or wear particles from the surface, could be introduced as a third-body abrasive between the belt and the sheaves.

$$V = KPS \quad (2.3)$$

$$V = \frac{KPS}{p} \quad (2.4)$$

$$V = \frac{KPS}{p^n} \quad (2.5)$$

Equations (2.3), (2.4), and (2.5) are the commonly used abrasive wear equations, equation (2.3) being the most general of the three. In these equations V is the volume of wear, P is the load, S is the sliding distance, and p is hardness. Again, K is the wear factor, which is determined empirically for individual wear situations, taking into account other factors such as the type of abrasive wear, the presence of lubrication, and other material properties. Equation (2.4) is the same equation used for single-cycle deformation and can be used when the wearing material is harder than the material being worn. Equation (2.5) is to be used in cases where repeated-cycle deformation abrasion is taking place. In this equation, n is a function of the difference in the hardness of the materials, as the difference in the hardness increases, the value of n increases [3].

In abrasive wear, asperity and particle size and shape have a large impact on the wear rates of materials. For two-body abrasion, the wear rates will decrease with time if the material that is removed collects between the protrusions of the abrasive surface, effectively changing the size of the protrusion until the surface is smooth and unable to continue causing wear. Naturally, the larger the protrusions are to begin with, the longer it will take for this phenomenon to occur. In many instances of mechanical wear, this is part of the break-in process. As the abrasive wear rate approaches zero, this does not

mean that wear will stop; it means that the mechanism of wear will merely change and possibly the overall wear rate will change as well.

The particle size and shape in three-body abrasion also plays an important part. The larger the particles are, the higher the wear rate. This may be due to any of several factors. For example, large grains are less likely to clog a surface, since they are able to create larger grooves by cutting or plowing, or they may simply be sharper than smaller grains. Although the exact reason for this trend is unknown, the evidence is strong that the relationship is linear. The number of abrasive particles does not play as important a part as one might think. As the number of particles decreases, the force pushing the particles into the surface increases; this tends to offset the fact that there are fewer particles to do the wearing by increasing the amount of wear the particles do. Overall, three-body abrasion tends to have lower wear rates than two-body abrasion, because the particles causing the wear are not fixed and are free to roll rather than slide, which causes cutting or plowing of the material being worn.

Because abrasive wear is most commonly single-cycle deformation, the micrographs of abrasive wear look similar to those shown in Figure 2-1 and Figure 2-3.

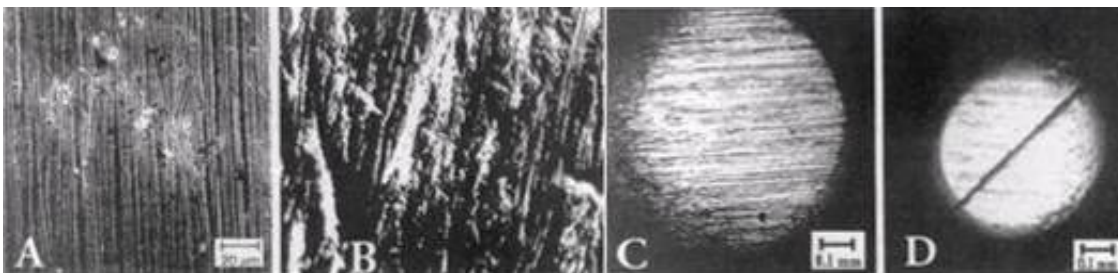


Figure 2-3 Examples of wear scars, in varying degrees, resulting from three-body abrasion [3].

Abrasive wear is a very strong candidate for the main mechanism of wear in a CVT. Because of the environment in which an ATV is typically operated and because the CVT is an open system not sealed from this environment, there is high probability for foreign particles to be introduced into the system during operation. These particles may act as a third-body abrasive or become lodged in the belt, causing a two-body abrasion. In addition to foreign particles, wear particles that have been removed from the substrate can also cause abrasive wear in the same way as foreign particles can.

2.3 Repeated Cycle Deformation

Dry sliding wear can cause repeated-cycle deformation; however, the effects of other wear mechanisms caused in dry sliding wear, such as adhesion, often eradicate the evidences of repeated-cycle deformation. Repeated-cycle deformation can happen under dry sliding, rolling contact, and impact loading, or any other condition in which deformation takes many cycles to occur. There are many mechanisms within repeated-cycle deformation, such as creep, compression set, and subsurface flow. The most common wear mechanism in repeated-cycle deformation is surface fatigue.

Surface fatigue is much like structural fatigue in that cracks initiate from a micro void coalescence and propagate until they meet the surface or other cracks, ultimately resulting in material loss in the case of surface fatigue or catastrophic failure in the case of structural fatigue. There are some key differences between surface fatigue and structural fatigue. For wear due to surface fatigue, or fatigue wear, the cracks are formed just below the surface; also, fatigue wear does not exhibit an endurance limit [4]. While

there is an incubation period in both fatigue wear and structural fatigue, fatigue wear is a continuous process in which the incubation is at different states at different depths beneath the surface. As the applied stresses become greater, the crack growth will start at a greater depth, allowing larger pieces to be removed.

The contact stresses play a very important role in fatigue wear. Because the deformation is occurring at the surface, micro-stresses as well as macro-stress should be considered. Macro-stresses are those stresses related to the apparent contact area, and micro-stresses are those related to the individual asperities contacting each other. Micro-stresses are relatively large compared to the macro-stresses at the surface, but they penetrate to only a small percentage of the depth to which macro-stresses penetrate. Two types of macro-stresses exist, conforming and nonconforming. Conforming contacts would be two mating flat surfaces, a cylinder in a hole of equal radius, or a sphere in a socket of equal radius. Nonconforming contacts would be a cylinder or sphere on a flat surface, a cylinder in a hole of unequal radius, or two parallel cylinders. According to Hertz contact theory, the greatest shear stress in nonconforming contacts will be at the midpoint of contact just below the surface [8]. This is important because it not only affects the normal stress distribution beneath the surface but also plays a role in the shear stress when a frictional force is added. Frequently, the shear force due to friction is neglected because it decays rapidly with depth; however, it plays an important role in fatigue wear. This shear force dictates the direction in which the cracks form. A normal load force will cause cracks to form perpendicular to the wear surface, and a frictional force will cause subsurface cracks parallel to the direction of friction. See Figure 2-4 and

Figure 2-5 for graphics of stress distribution and crack formation under the influence of different stresses.

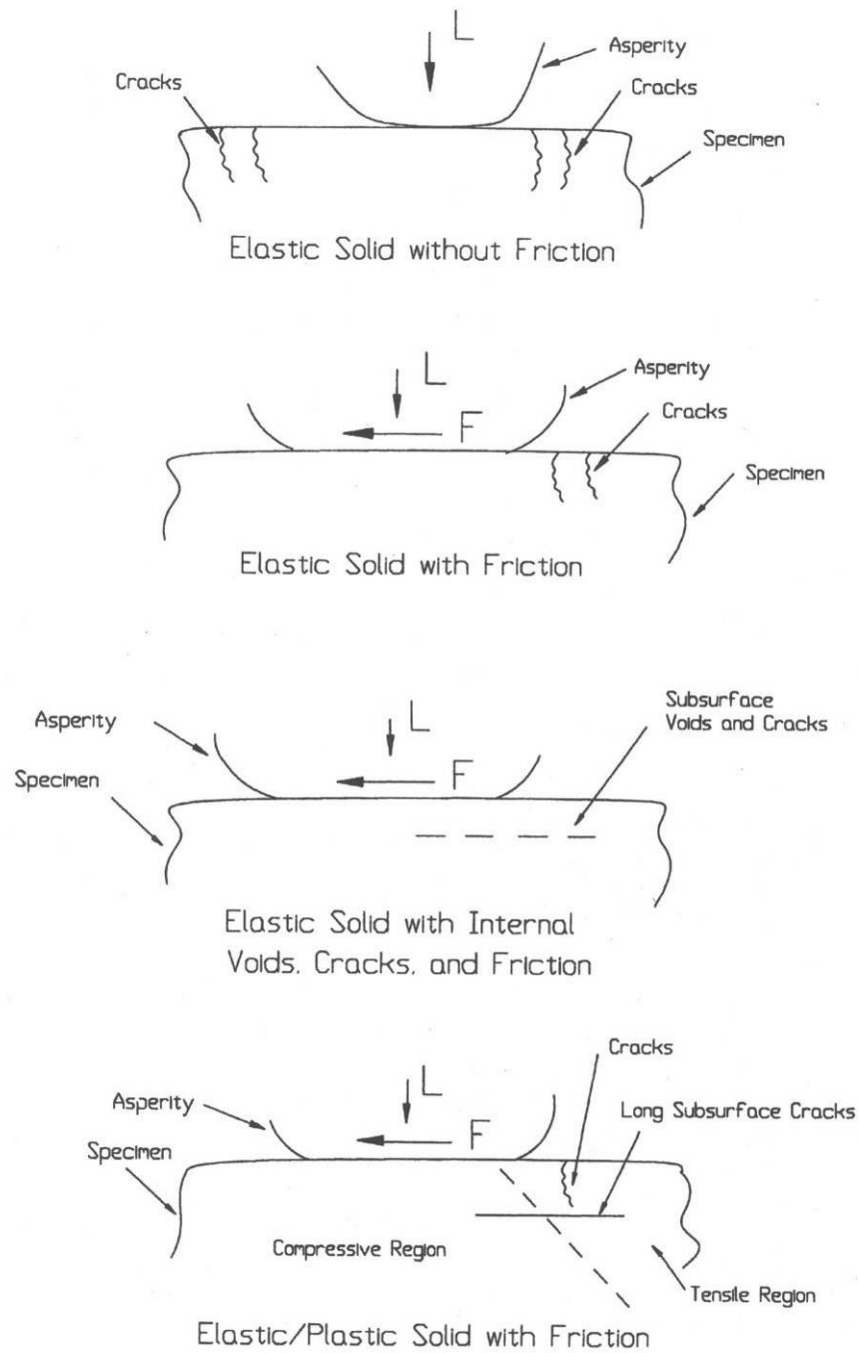


Figure 2-4 Examples of the influence of the nature of stress system on crack formation [3].

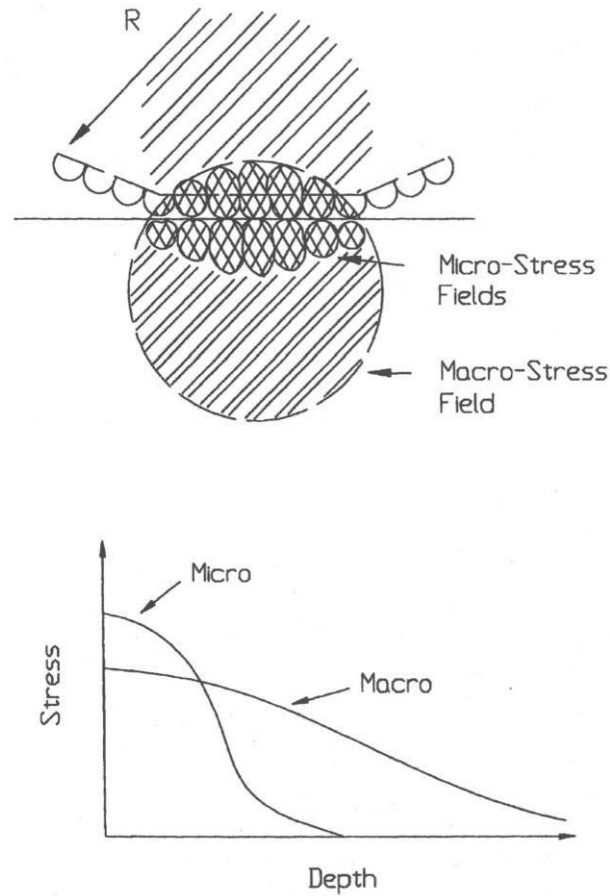


Figure 2-5 General nature of the stress field in contact situation, illustrating the relative effects of contact geometry and asperities on stress[3].

Many models of fatigue wear have been proposed. The most commonly used are those based on Wohler's equation for fatigue, but there have been models developed based on dislocation theory and fracture mechanics. As with the equations used to describe other mechanisms of wear, the equations used to describe fatigue wear have terms that must be determined empirically through testing. Equation (2.6) is one of the general equations used for fatigue wear; different variations of this equation could be used depending on some of the assumptions of the asperities and types of contact.

$$V = KP^n S, \quad n \geq 1 \tag{2.6}$$

In this equation, P^n in the power relationship, where n is usually close to one but in some cases can be as high as six. Again, K is an empirically determined term and is dependent on material properties, contact parameters, and the mode of stressing, but not directly dependent on the hardness. The variable S is the sliding distance, number of revolutions, or number of impacts, depending on the type of wear [3].

Sliding surface fatigue generally progresses through three stages of wear scar morphology. In the first stage of fatigue, wear micro striations appear similar to those in single-cycle deformation. The material is plastically deformed but no material is lost. The second stage shows deformation perpendicular to the movement, or cross hatching. This is evidence that more than single-cycle deformation is occurring. The first two stages constitute the incubation period, because no significant material is lost. Stage three is the beginning of material loss. The crosshatching features become more definite and spalling and flaking occur. Figure 2-6 shows this process for a hardened steel sphere sliding on lubricated single-crystal Copper, where stress levels were kept well under the yield point of the Copper. It is important to note that although sliding fatigue wear may follow the same general pattern, the wear scar morphology may change significantly with different materials and stresses [9].

In rolling and impact fatigue wear, wear scars tend to be much larger, even on the macroscopic level. These wear scars are usually pits of various sizes formed by large particles being removed. Examples of rolling contact wear scars are shown in Figure 2-7.

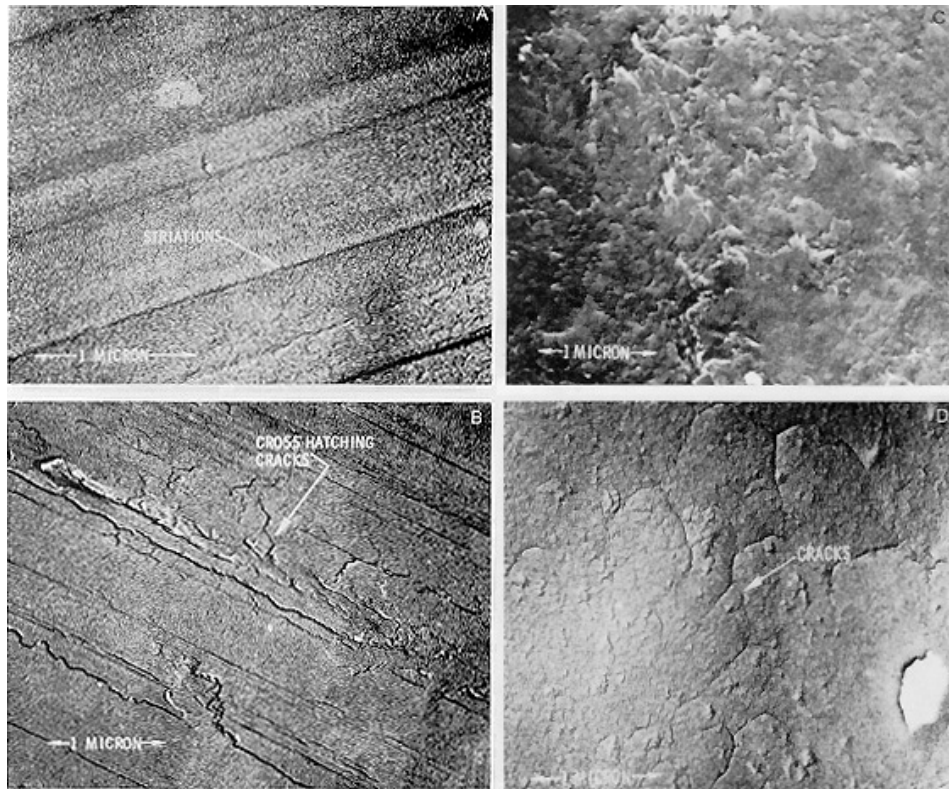


Figure 2-6 Wear scar morphology of single-crystal copper in lubricated sliding [3].

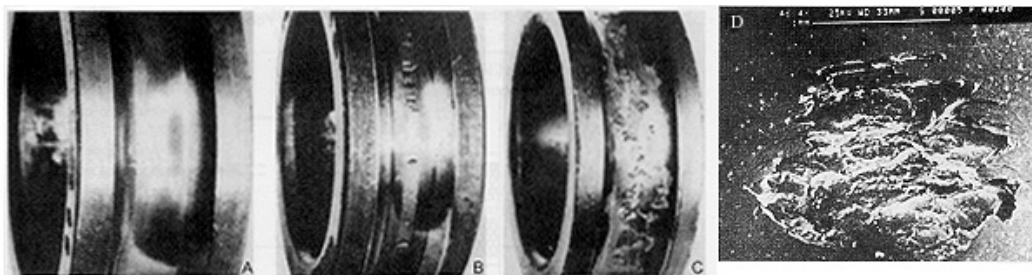


Figure 2-7 A - C Shows the progression of severe rolling contact wear. C shows normal rolling contact fatigue wear scar [3].

Fatigue wear in the CVT is highly likely. The CVT goes through many millions of cycles during its lifetime. During these cycles, it is under both a normal, and

sometimes a very high shear force. The contact type is a nonconforming contact; however the loading type does not follow any of the standard types. The CVT has rolling contact loading components because there is a cyclical normal force. It also has a sliding component because of the frictional force used to transfer the torque. This makes deriving a fatigue wear equation for the CVT difficult, because these components are neither true rolling nor sliding contact forces.

The wear behavior of the CVT is extremely complex. There are many different mechanisms of wear taking place, and most of these mechanisms do not fit the assumptions made for the established wear models.

2.4 Wear Behavior of Aluminum and Coated Aluminum

As previously stated, the CVT is made of A390 die-cast aluminum. Parts are often made from aluminum because of its castability, density, thermal conductivity, or look; however, it is rarely, if ever, used for fatigue or wear properties. Most alloys of aluminum have relatively low hardness and tensile strength, which are typically very important factors in wear, as discussed in the previous sections of this chapter, but it is used in wear applications because of its other desirable properties.

2.4.1 Aluminum in Wear Applications

In order to better understand the dry sliding behavior of aluminum alloys, an experiment was conducted to test the feasibility of using aluminum pulleys with a steel cable [10]. This test used a pin-on-disk wear test, with one test conducted using an aluminum pulley and steel cable to verify results of the pin-on-disk test. In this test, aluminum exhibited work softening. In order to determine the wear mechanism, micro-

graphs were taken with both an SEM and an optical microscope. The aluminum showed signs of adhesive wear to some degree in all of the alloys. Additionally, the softer alloy had severe abrasive wear, and the harder alloys showed fatigue wear; see Figure 2-8 for micrographs of these types of wear.

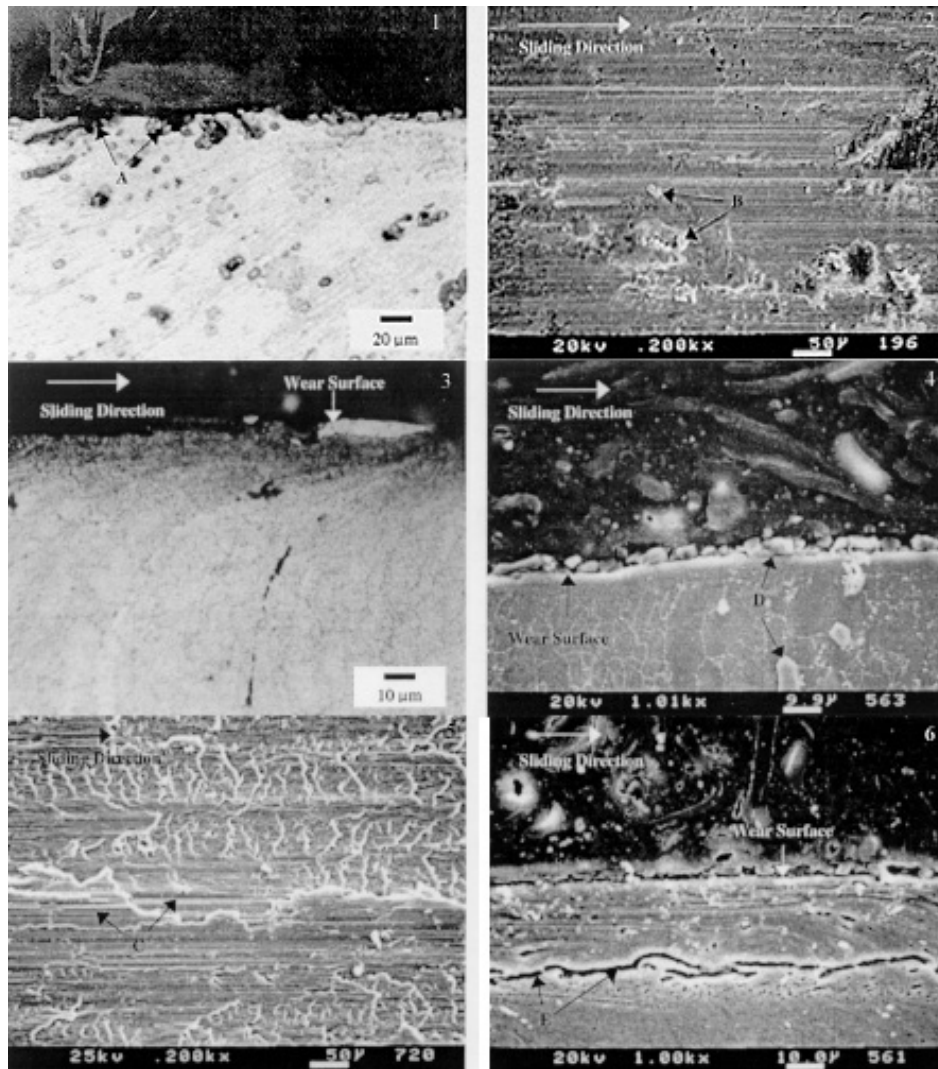


Figure 2-8 (Previous Page): 1) Cross section of a 2014-T6 sheave wheel specimen indicating adhesive and abrasive wear 2) Wear Surface of 2014-T6 sheave wheel specimen indicating abrasive wear (grooves) and wear particles at B 3) Cross section of a 2014-T6 specimen indicating adhesive wear (lines of shear induced plastic deformation) 4) Cross section of a 2014-T6 specimen revealing aluminum-oxide particle formation at D 5) Wear surface of a 2014-T6 specimen indicating adhesive wear (galling) and abrasive wear (grooves at C) 6) Cross-section of 7050-T7451 specimen indicating adhesive wear (lines of shear-induced plastic deformation with void formation and coalescence at E) [10].

Another study on aluminum alloys 5052 and 5083 was conducted to understand the effects of strengthening aluminum by creating ultra-fine grains in the material to improve wear [11]. The study produced ultra-fine grains in the two aluminum alloys and compared the wear rates with the alloys of standard grain size. The ultra-fine grain alloys had a higher wear rate despite the greater tensile strength and hardness. This shows that hardness and tensile strength are not always the dominant factors in the wear resistance of a material.

2.4.2 Wear Coatings

Several coatings have been developed in order to increase the wear resistance of many materials. These coatings vary depending on the coating material, the substrate material and the process used to deposit the coating. Most of these coatings have been developed for steel, but there are many that can be applied to aluminum and other materials. Coatings that are often used for wear are hard chrome, electroless nickel metal, hard coat anodizing, and flame sprayed metal. Hard chrome being the most commonly used coating for wear resistance [12]. One example of this is hydraulic cylinder rods which are often heavy chrome coated because of the wear resistance of the coating and its low coefficient of friction. Electroless nickel metal is often used on parts where corrosion and wear resistance are important. Hard coat anodizing is often a good method for increasing the wear resistance of aluminum parts. Aluminum is often hard coat anodized, because other electrolytically deposited coatings do not always adhere well to the aluminum substrate. Other surface treatments such as shot peening can be used to

increase the wear resistance of a material along with many new coatings and treatments tailored for specific applications [13].

2.4.3 Wear Behavior of Coated Aluminum

Aluminum is the material of choice in many applications, especially those where weight and thermal conductivity are important. It is often used for its light weight or high thermal conductivity despite its poor wear characteristics. This is where coatings that increase the wear resistance, but do not affect the other properties of the base material are very beneficial. Because the surface hardness, surface finish and other factors affecting wear are changed by coating a part, it becomes important to understand the change in the part wear behavior using the coating.

To better understand the wear behavior of coated aluminum, a study was conducted to observe the wear behavior of CrN coated aluminum alloys [14]. This study used an unlubricated ball-on-disk wear tester. The ball that was used was polycrystalline alumina. The CrN coating increased the surface hardness of the 6061 and 7075 alloys nearly 6.5 times relative to their respective initial hardness. The coefficient of friction was higher for the 6061 coated alloy than for the 7075 coated alloy. The results and conclusions of this study showed that the 6061 coated alloy had much higher wear rates. This was in part because at high loads, the coating would be scraped off early in the process. As the load increased for the 7075 coated material, the wear rates actually decreased. This is explained by the higher coefficient of friction in the 6061 coated alloy and the higher strength substrate of the 7075 alloy. Thermal softening and plastic fracture was observed in the 6061 coated alloy, while fatigue wear was the mechanism of wear in the 7075 coated alloy.

In the study conducted by Michael Whiting, the effects of hard coat anodizing on the wear resistance of A390 die-cast aluminum also showed that hardness is not the only factor to be considered in wear resistance of a coating [1]. In this study, a modified Taber Abraser test was used to determine the wear rate of uncoated and coated A390 aluminum. The hard coat anodized part had a larger wear rate than the uncoated part. It was concluded that because of the more brittle and porous surface of the hard coat anodized part, surface fatigue and abrasive wear were accelerated.

2.5 Wear Hypothesis

It is hypothesized that multiple mechanisms of wear are contributing to the wear of CVT sheaves. These mechanisms include single-cycle wear in the form of adhesion and abrasion and repeated-cycle wear in the form of abrasion and surface fatigue, surface fatigue being the dominant wear mechanism. This is believed because the belt of the CVT slips a relatively small amount compared to the amount of time that it is not slipping. Slipping is required for both two and three body abrasion. Because of the large differences in tensile strength between the belt and aluminum, adhesive wear is not thought to be a major contributor to the wear problem.

As demonstrated by the examples in the previous section, wear rates of materials cannot easily be predicted. In most cases, wear rates and mechanisms of wear must be determined by experimentation before the wear models can be used to predict wear. In order to test the above hypothesis, experimentation will be conducted as outlined in chapter 3.

3 Methods and Procedures

Premature wear of CVTs is a significant problem. As discussed in chapter 2, there are many factors that affect the wear of a mechanism. In the case of a CVT, changes made to improve the wear characteristics must be carefully chosen based on what is known about the wear mechanisms associated with a CVT. At the same time, the changes must not adversely affect the performance or unreasonably increase the cost of the CVT. Typically the method used to increase the wear resistance of a mechanism is to change the material of which it is made. A CVT made of steel would wear substantially longer but would not be practical, because the increased mass of a steel CVT would adversely affect its performance due to its increased rotational inertia. If a material with equal density and higher strength, such as high strength aluminum or titanium, were to be used, it would unreasonably increase the cost of the part. Changing the loads the CVT experiences to reduce wear would also be an unacceptable solution because of customer demands for performance. Because of the design requirements of CVTs, coating the sheaves with wear-resistant coatings is the hypothesis that was chosen to pursue. As discussed in chapter 2, the K factor in most wear equations must be determined empirically for each wear scenario. Because a K value is not already established for the CVT wear scenario the problem could not be modeled making it necessary to test each method for improving the wear resistance.

This chapter will discuss the methods and procedures used to create and evaluate the wear of a primary clutch. First the proposed solutions to the wear problem will be discussed, followed by the development of the wear test stand and wear test procedure. Finally the methods and procedures for evaluating the wear will be explained.

3.1 Proposed Solutions to the Wear Problem

Wear-resistant coatings have been developed for many different applications and materials. In the case of a CVT, it is important that the coatings chosen be appropriate for this wear application. The criteria used to determine appropriateness of a coating for a CVT are:

- The coating must bond well with the aluminum substrate
- The coating must have a similar coefficient of friction to standard machined aluminum
- The coating must have sufficient wear-resistant properties for the types and amounts of wear that will occur in the CVT
- The coating must be cost effective for application in a high production application.

As discussed in chapter 2 the shear stress resulting from the frictional load will be the greatest near the surface. Because of this high shear stress, the bond strength of the coating is critical to the wear resistance of the coating. If the coating does not bond well to the substrate, the wear will be accelerated instead of reduced because abrasives will have been added to the system. The coating must also have a similar coefficient of

friction to the standard machined aluminum in order to maintain the shift characteristics of the CVT and to transfer adequate torque to the wheels.

With today's technology, coatings can be highly tailored to perform in different wear applications. As discussed in chapter 2, the factors that determine wear rates can vary greatly with different wear mechanisms and the wear materials themselves. As a consequence, careful consideration in choosing a coating for testing was important. The coatings to be tested were chosen because they perform well under wear mechanisms of those found in a CVT. For example because of the hardness of the coatings they often perform well in abrasive environments. Because of the high volume production of CVTs, it is very important that the coating can be cost-effectively applied to the aluminum sheave material in a production environment [15].

3.1.1 Coatings and Coating Processes

After careful consideration of the criteria in the previous section, the coatings in Table 3-1 were chosen to be tested. The sponsors of this research have deemed the suppliers of the coating information in this section proprietary; therefore, the suppliers will not be disclosed or referenced.

Table 3-1 Tested coatings and their coating process

Electrical Deposition	Other Deposition
Hard Coat Anodized	Composite Ceramic
Hard Chrome	Electroless Nickel

Electrical deposition plating is widely used to coat metal parts in production. Anodizing is often included as a type of electrolytically deposited coating even though no material is being added to the part. Anodized coatings vary in purpose from decorative coatings to wear-resistant coatings, but the processes for creating the anodized surface and depositing a material are generally very similar. Electroless coating is similar to electroplating except uses a chemical catalyst to cause the plating material to bond to the substrate instead of electricity.

Typically every electrical and chemical plating processes use three stages: pretreatment, coating, and post treatment. The pretreatment is usually a process that is used to clean or etch the metal surface. It is very important that any oil, dirt, or oxide removed the surface. If the impurities are not removed, the coating will not bond well to the surface. In order to get the surface clean, strong acids are often used.

After the surface has been sufficiently cleansed, the part is put into a tank filled with a solution of the coating material. The solutions used in this step of the process are often proprietary, because they determine the properties of the coating. Once the part is in the tank, an electrical current is applied for electroplating through the tank with the part acting as a cathode. Because the part is negatively charged, the positively charged metallic ions will be attracted to and bond with the part. It is in this step that anodizing differs. In anodizing, instead of a metallic ion bonding to the part, the solution contains a chemical that causes the surface to oxidize when the current is applied. The amount of material or thickness of the oxide layer that is deposited on the part is dependent on the current and the time the electrical current is allowed to flow. In chemical deposition

catalysts and many other additives are used to cause the metallic ions to bond to the substrate [16].

Once the part has the desired coating thickness applied, the part usually goes through a post treatment process. This process can vary as much as the coating. Most coatings will require a sealant to fill micro-cracks or to stop further oxidation. Sometimes a mechanical buffing or polishing process will be used to achieve a desired look or surface finish. The part may also be heat treated, depending on the required properties and the coating material used.

An electroless nickel metal coating is a chemically deposited coating that was tested as a wear resistant coating for CVTs. This nickel coating has many similar properties to chrome coating. It has a very shiny appearance and is very wear and corrosion resistant in the applications which it has been tested. It has a plated hardness of 63 Rockwell C and can be heat treated to further increase the strength of the coating and substrate. This coating can be deposited up to 0.001 inches thick. This coating was chosen because, unlike a chrome coating, it does not leave micro voids and micro cracks on the surface. Electroless nickel metal will likely be the more expensive solution, but may offer increased performance because of its higher coefficient of friction. This coating is also supposed to adhere better to the substrate than hard chrome.

A variation of a hard coat anodized coating was tested. The hard coat anodized coating used differs from standard hard coat anodized coatings because it is impregnated with PTFE particles, which increase corrosion and abrasion resistance. This coating has a hardness of 65 - 70 Rockwell C and can have a thickness of .0008 - .003 inches. This coating was chosen for testing because of its bond strength with the substrate surface and

its very high hardness. Because CVT sheaves are made from A390 die-cast aluminum, which has a very high silicon and copper content, it is difficult to get most coatings to consistently bond well with the substrate. However, because this is an anodizing process, the coating is much more reliable. The major drawback to this coating is that it tends to yield a relatively porous surface, making it more susceptible to surface fatigue.

The hard chrome coating is the third electrolytically deposited coating that was chosen to be tested. This coating is a chrome hybrid coating that, in tested situations, provides very good wear and corrosion resistance. This coating is applied in thicknesses of .0001-.0003 inches and has a hardness of 66 - 70 Rockwell C. This coating differs from other chrome coatings because the micro cracks formed in the coating process are much smaller than those formed in the standard chrome coating process. This coating is also one of the less expensive coatings. One of the drawbacks of this coating is that it cannot be applied as thickly as the other coatings and does not always bond well to a die-cast aluminum substrate. Additionally, because of the micro cracks of the chrome, part of the test procedure will be to determine the necessity of a post polishing or buffing process to stop excessive belt wear.

Unlike the hard chrome and electroless nickel metal coatings, the composite ceramic coating is not an electrical deposition or chemical deposition coating. Because the composite ceramic is a water deposition coating it will not have the micro cracks associated with the other coatings. This coating also has unique heat management qualities that may reduce the chances of burning or glazing a belt.

Water deposition is a process in which the coating is sprayed on in a solution with water and then baked on. Until this research this coating has mostly been used in heat management applications.

3.2 Test Procedures

The testing consisted of two stages: The first stage of testing was used to better understand the behavior of the CVT as it works on an ATV. Because there is no available model for a CVT, these tests were necessary to predict the optimum settings for use in the second stage of testing. The second stage of testing was conducted to create wear on the CVT and measure changes in shift characteristics that come with wear. In addition to measuring the changes in shift characteristics that occur as the clutch sheaves wear, the volume lost due to wear was measured periodically throughout the duration of the test. This volume measurement of wear was done to determine the wear rates of the stock aluminum clutch sheaves as well as the coated sheaves. Wear was also evaluated during the second stage of testing by using a chassis dynamometer to test the performance change between worn and unworn clutches.

3.2.1 First Stage Tests

As previously stated, the objective of the first stage of testing was to observe the behavior of a stock CVT in different loading conditions and to determine the optimum conditions in which to create wear. The two most important factors determined in this testing were the rpm at which the primary clutch should spin and the load that should be applied to the secondary clutch. The higher the rpm of the primary clutch, the higher the clamping force on the belt. At certain speeds and loads, the belt will experience slip in

the drive clutch. If the slip is great, the belt will heat up and melt at the contact point of the sheaves, ruining the belt. Obviously, this is undesirable. If the speed of the primary clutch is too low or the load is too low, then the belt will not ride in the position in which wear most often occurs and may take too long to create a significant wear groove.

In order to determine the proper rpm and load for testing and to observe the CVT under different loading conditions, a test stand was built. The test stand (see Figure 3-1) consisted of a Polaris, 2006 Sportsman 500, fuel injected, 4-wheeler, modified so that a hydraulic resistance system could be attached to the rear axle. This was done by removing the rear wheel and bolting a sprocket in place of the wheel. The sprocket then was connected to the hydraulic pump using chain drives to achieve the proper speeds. The resistance system consisted of a Haldex cast-iron 1.8 in³ displacement hydraulic gear pump, a needle valve to control pressure, an oil-to-water heat exchanger to dissipate the heat generated in the needle valve, and a reservoir tank. The hydraulic system used a SAE 10w or ISO 32 hydraulic fluid (see Appendix A for data sheet).

There was also data acquisition for the system. The pressure was read on the high pressure side, and the temperature was read on the both the high pressure side and the low pressure side. The pump and the engine rpm were also being monitored. Labview™ and a National Instruments® SCXI chassis and data acquisition card were used to monitor the pressure, temperatures, and pump rpm. Flow rate, torque, and horsepower were also calculated in Labview. The engine rpm was observed on the 4-wheeler's tachometer.



Figure 3-1 First stage test stand.

The hydraulic resistance system used the positive displacement pump to create a constant volumetric flow, regardless of the pressure of the system. The needle valve controlled the resistance of the flow, and proportionately the pressure, of the oil flowing from the pump. As the resistance and pressure rise, the torque needed to turn the pump increases, increasing the load on the CVT. As the pressure across the needle valve drops, the temperature rises; this rise in temperature is why the heat exchanger is needed.

The test procedure of the first stage test stand was to manually hold the engine rpm constant with the throttle while adjusting the hydraulic pressure to a set point and observing the behavior of the CVT. See Table 3-2 for tested values that yielded a transition between slipping and no slipping. At these values, the CVT was in its lowest ratio.

Table 3-2 First stage test values

Engine RPM	Tested Pressure	Comments
3900	1000 psi	Gross slipping occurs
4200	1250 psi	Little slipping occurs
4500	1250 psi	No observed slipping
4500	1750 psi	No observed slipping

With the data collected in the first stage testing, specifications could be made for the second stage test stand.

3.2.2 Second Stage Test

The second stage test stand (see Figure 3-2) was built to do the actual wear testing at an accelerated rate compared with normal ATV use. With the information from the first stage test stand, it was determined that the primary clutch should spin at approximately 4500 rpm, and the stock blue spring in the drive clutch should be replaced with a longer, white spring. This would allow the drive clutch to run at near full engagement, thus allowing for maximum torque transfer with only minor slipping. The motor used to drive this test stand was a 50-horsepower, 3-phase ac induction motor that ran at 3460 rpm at 60 Hz. A Goodyear Eagle Pd® synchronous belt with offset helical teeth was used to transfer power from the motor to the primary clutch. A 50-tooth sprocket was used on the motor and a 38-tooth sprocket on the primary clutch drive shaft, resulting in about a 1.3 ratio, which spun the primary clutch at approximately 4600 RPM.

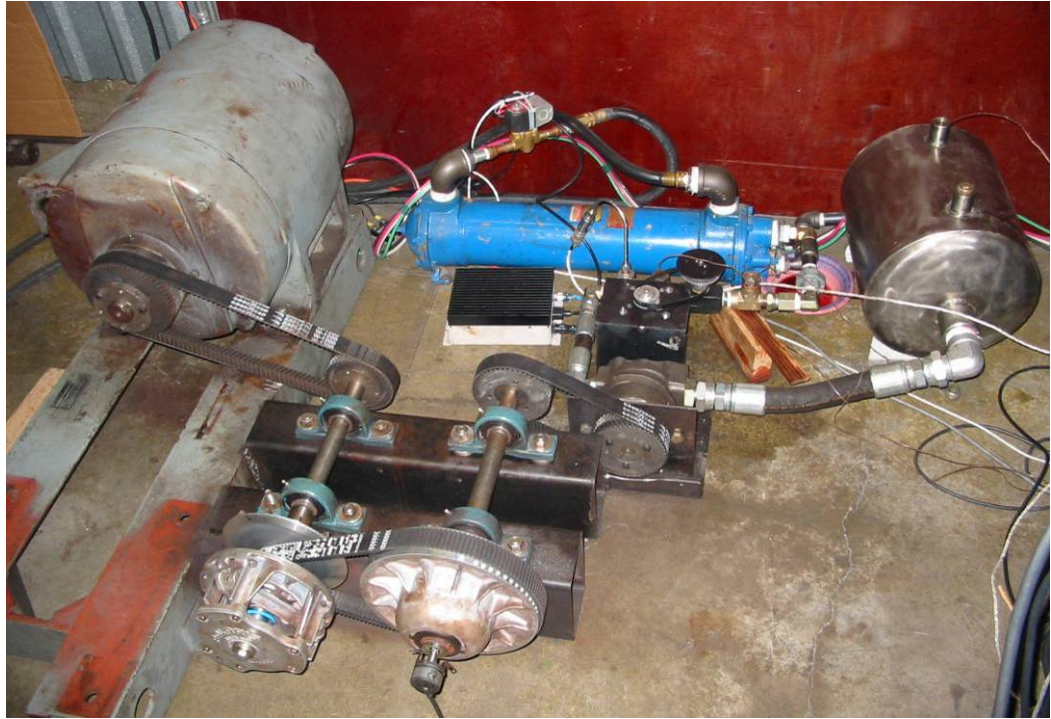


Figure 3-2 Second stage wear test stand.

The CVT was mounted to drive shafts designed for running a CVT on a test stand. Pillow blocks were used to fixture the drive shafts to a rigid metal frame. This frame supported all of the major drive and driven components of the test stand. The secondary clutch used a similar synchronous belt drive to drive the pump with a one-to-one ratio. With this ratio, the pump would operate between 1160–2800 RPM depending on the load applied to the CVT. This test stand used the same hydraulic resistance system as the first stage test stand.

Because this test stand needed to run for long periods of time unattended, it was fully automated. Like the first stage test stand, pressure, temperature, and pump rpm were being monitored with Labview and a National Instruments SCXI chassis. In the second stage test, however, several controls were added using Labview software and

National Instruments hardware. The main drive motor was controlled used a solid state relay, a mechanical relay and an additional power supply to power the relay. Connected to the same relay and power supply was a solenoid valve that would turn on and off the water to the heat exchanger. If the main drive motor was on, water would be flowing through the heat exchanger, reducing the chance of overheating. The most important control that was added was the needle valve control. A stepper motor was mounted to the frame and the needle valve was fitted with a sprocket so it could be driven by the stepper motor. The stepper motor was controlled using Labview and the SCXI chassis. In addition to these controls, a camera was setup to watch the test stand so it could be observed remotely.

The Labview front panel (see Figure 3-3) was the interface for the controls of the test stand. The Labview program (see Appendix B for Labview block diagram) performed many functions, including running test cycles and monitoring the system for failures in the stand. To run a cycle, a high pressure was defined and a duration was set for the test stand to run at that pressure. A second, lower pressure was entered and a duration define for the test stand to run at that pressure. The second pressure serves two purposes. If the belt remains at one position for an extended period of time, belt compound may begin to build up on the clutch sheaves causing a performance change in the CVT which could be confused with the performance changes due to wear. This lower pressure also allows the CVT to shift from a low gear to a high gear and back to a low gear. It was during these transition times that changes in shift characteristics could be observed. Usually the time that the stand runs at the lower pressure is only about a fifth of the time of the time that it runs at the higher pressure.

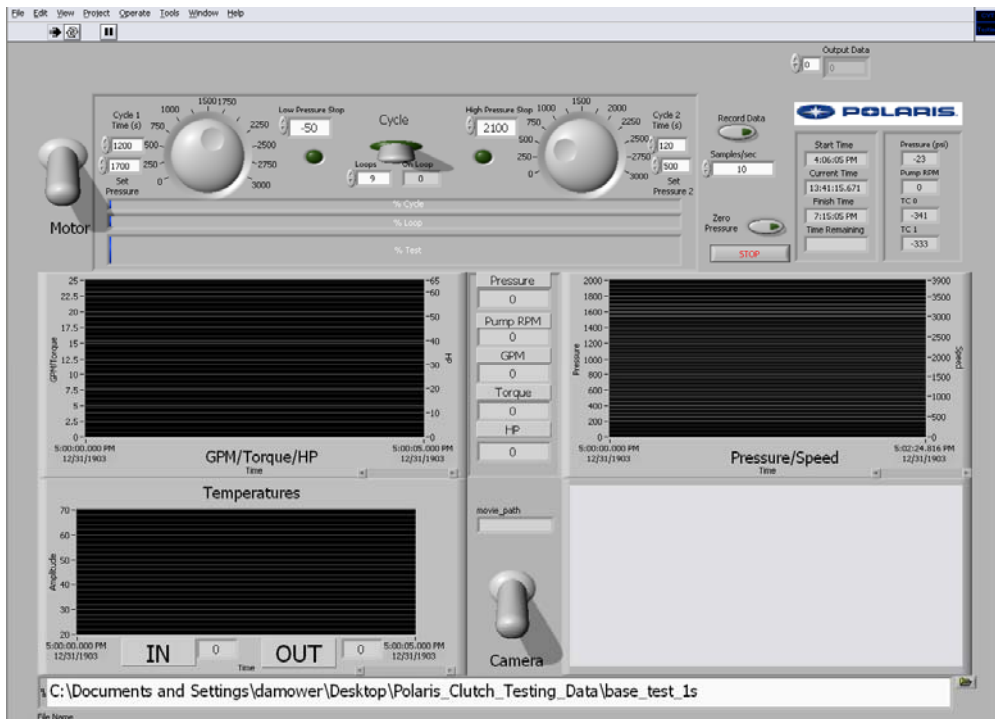


Figure 3-3 Labview front panel for second stage test stand.

To run a test, the operator would input the number of loops two defined pressures were to cycle through for a total test time. When the cycle was started, the program would read the pressure if the pressure was not within a defined region of the set pressure, the program would adjust the needle valve accordingly. The program and data acquisition took data on a continuous basis in order to maintain a pressure in spite of changing viscosity and other environmental factors.

Also entered into the program were the over-pressure and under-pressure points. These points are safety stops if the pressure exceeds the set high pressure point or drops below the set low pressure point, the test stand will shut down. Labview also has a

Webcasting feature, enabling the program to be controlled remotely from any computer with an Internet connection.

Procedure for Running Wear Test Stand

1. Mark a new stock primary clutch on the top plate, Spider, fixed sheave, and movable sheave. Marks should be made in a line so the clutch could be properly realigned during reassembly. See Figure 3-4 for example.
2. Disassemble the clutch and clean sheaves with alcohol and paper towels.
3. Measure the surface of the fixed and movable sheaves. See measuring procedure for details.
4. Reassemble the primary clutch, aligning marks made in step one. Replace the stock blue spring with white spring. Put the primary clutch on the test stand. Mark a belt to correspond with the label on the clutch.
5. Run twenty-five hours of tests in three to seven hour increments with the high pressure set at 1900 psi for 1200 seconds and low pressure set at 400 psi for 240 seconds.
6. Inspect CVT and test stand for abnormalities between tests. Record test in lab book note any problems or abnormalities. Check data file of recorded cycle data; note any changes in shift behavior of the CVT. Measure and record belt wear.
7. Conduct performance test. See performance test procedure for details.



Figure 3-4 Labeled primary clutch.

Following this test procedure allowed for accelerated wear to occur. The torque that the CVT is transferring under these conditions is approximately 45 ft-lbs, whereas a Polaris Sportsman 500 is capable of producing only 27 ft-lbs of torque at 4600 RPM, the speed of the primary clutch.

3.2.3 Procedure for Measuring Results

The procedure for measuring the wear volume uses a Hommel Tester T8000 profilometer made by Hommel_Werke (see Figure 3-5 for layout). The software used to run the profilometer and analyze the data was the Turbo Rauheit v6.14 (see Appendix C for technical specifications of hardware and software).



Figure 3-5 Hommel Layout

The Hommel profilometer uses a stylus to record the profile of the surface of a part. As the stylus moves across the part, data containing information about the surface roughness and surface waviness is calculated and recorded. Surface roughness is an evaluation of surface topology looking at changes in height over very small distances parallel to the surface. Surface waviness is an evaluation of surface topology looking at changes over a larger distance parallel to the surface [17]. The software also allows for analysis of the profile. One of the many features available in the analysis suit is air area calculation; this is the feature that was used to calculate the amount of wear. The feature is used by selecting two points on the profile then software draws a straight line between these points and calculates the area above the profile enclosed by the lines. The operator

had to use good judgment in choosing the areas which should be counted as wear area. Although most of time the distinction was clear sometimes it was difficult to know which areas should be defined as wear areas. In addition to wear area, surface roughness values were recorded and statically analyzed for trends.

The following was the procedure used for measuring the amount of material lost and the surface roughness of worn and unworn primary clutches. This procedure was used at step 3 of the wear test procedure then again at the end of the 25 hour test.

Procedure for Measure Amount of Wear

1. Start Turbo Rauheit software. Load CVT measuring program. Program should have the following setting.
2. **Be very careful not to bump or touch stylus.** If not already, raise stylus and place sheave on the fixture plate. Use level and blocks to level one side of the sheave. Tape may be required to keep sheave in place.
3. Lower stylus to position shown in Figure 3-6. Make sure that the sheave is in a position the stylus will be able to make a 15 mm pass.
4. Zero the stylus and begin the scan. Watch screen to ensure the stylus stays within range if not raise stylus and make adjustments using step 2.
5. Once scan is complete go to measuring screen save the profile and record values for Rq, Rt, Ra, and Rz on Surface data spread sheet.
6. Open profile analysis screen turn on W filter and cross hairs.
7. Using the cross hair points on the W filter line define the wear area then select calculate air area. Paste measured area on the screen.

8. Use Ctrl Print Screen command to copy profile and area measurement to sheet 2 of surface data spread sheet. Label image with sheave information.
9. Record any comments about sheave condition and repeat process for other sheave.

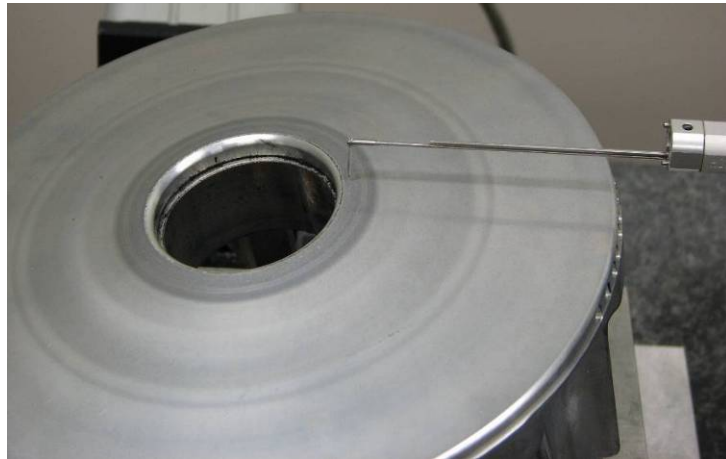


Figure 3-6 Start point for stylus

3.2.4 Methods and Procedure for Measuring Performance

A designed experiment was used to measure performance changes in the CVT between new and worn primary clutches. A chassis dynamometer was used to take these measurements. Several runs with new and worn clutches were conducted, and the acceleration curves of the runs were compared for performance changes. Four runs were conducted at minimum, medium, and maximum loads. For each of these runs the load was set and then full throttle was applied until the maximum speed for that load was reached. To compare acceleration runs at a load, the speeds were plotted versus time for the worn and new clutches, see Figure 3-7 for example of plot.

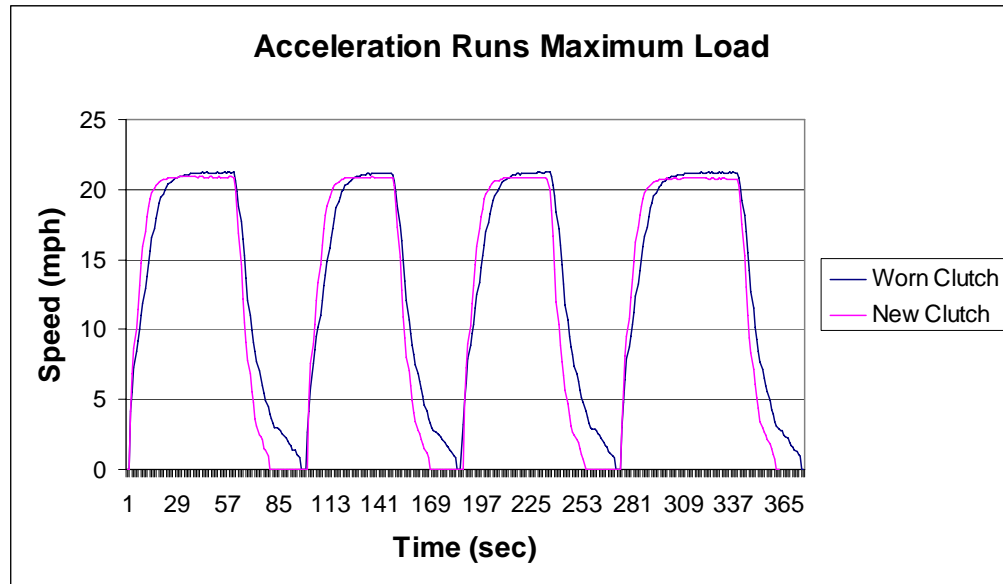


Figure 3-7 Example acceleration plot.

New primary clutches were tested and after 25 hours on the wear test stand the worn primary clutches were tested again. This test was also used as a prescreening test for the coatings. If a coating performed significantly worse than other coatings or failed altogether, then it was eliminated.

Procedure of Dynamometer Testing

1. Tie down ATV as shown in Figure 3-8. First tighten the forward straps to ensure adequate tire contact with torque roller.
2. Bolt on primary clutch to be tested (follow the run order) and install the dyno-belt. Note, putting ATV in neutral will help with this step. The dyno-belt should be used, not the belt used on the wear test stand. If the dyno-belt is excessively worn then it should be replaced with a new belt.

3. Shift ATV into high gear and rev engine to seat belt.
4. Start Labview VI for dynamometer. Name file for data to be written to. The file name should reflect the clutch and load that the test was run.
5. While full throttle is applied to the ATV adjust the load to min mid or max. Min is the minimum load the dynamometer could apply, the mid setting was a load such that the top speed was 37 mph, and the max setting was the maximum load the dynamometer could apply.
6. At each load, start recording data and run the AVT to top speed with full throttle four times.
7. Stop recording data after the fourth run. Change the data file name to reflect next load. Repeat steps 5 and 6 for until all loads have been run.
8. Repeat steps 2 - 7 for all clutches.



Figure 3-8 Dynamometer testing

Matlab program was used to evaluate the acceleration curves created during the dynamometer testing. Microsoft Excel was used to do a statistical analysis of the acceleration curves.

3.3 Determining Dominant Wear Mechanism

Many different mechanisms of wear are taking place in the CVT. It is very important that the dominant mechanism of wear be identified, not only in the tested clutches, but also in the warranty return clutches provided by Polaris. As stated in Chapter 2, the most common way to determine the dominant wear mechanism is by analyzing the wear scars and wear morphology of the wear surface. This was done using a stereo optical microscope and a scanning electron microscope (SEM).

The stereo optical microscope could be used during testing to make observations of wear scars. However, because of the limited magnification of the stereo microscope the SEM was needed. Since the SEM requires a vacuum chamber to operate and a whole CVT would not fit in the chamber smaller samples needed to be cut from the sheave to be analyzed. Because the primary clutch had to be destroyed in order to fit in the vacuum chamber, only completely worn clutches were analyzed in the SEM. Micrographs of the stock tested clutches were then compared to the micrographs of the warranty returns to confirm that the same type of wear was taking place. These micrographs were then compared to micrographs in textbooks and technical papers to determine the dominant types of wear.

3.4 Summary of Testing and Methods

The testing can be divided into two groups: those process that produces wear and those methods used to evaluate the wear. The second stage test stand produces the wear by running the CVT through a loaded and unloaded test cycle, where a majority of the time is spent at a high load.

The test stand is also used to evaluate the wear of a CVT. As the test stand goes through loading and unloading cycles, the change in shift characteristics can be seen by plotting the rpm of the secondary clutch versus the torque applied to the CVT. Wear is also measured with a Hommel Tester T8000, profilometer and Turbo Rauheit v6.14 software package is used to estimate the volume lost due to wear. From this estimated volume loss, wear rates can be established by dividing the loss by the amount of time required to achieve the loss. Finally, changes in performance are evaluated using a chassis dynamometer and plotting both the new and worn CVT acceleration curves on the same graph. In addition to the actual wear and the performance, the main mechanism of wear was determined by comparing micrographs of wear scars on the worn sheave's surface with micrographs of warranty return clutches and textbook examples in chapter 4.

4 Results

This chapter includes test data and some discussion of that data. Section 4.1, Wear Test Stand Results, explains how the data from the wear test stand was interpreted to show the change in shift characteristics of the CVT as wear grooves developed. Section 4.1 also summarizes the data from the wear test stand for the stock and coated clutches. Section 4.2, Dynamometer Results, shows the results of an experiment designed to evaluate the performance changes in the CVT as a result of wear. Section 4.3, Wear Measurement Results, shows the volume lost due to wear and wear rates of the stock and coated clutches. Section 4.4, Scanning Electron Microscope scans, shows wear morphology and wear scars which developed during testing.

Clutches referenced throughout Chapter 4 are labeled with the following method. Each coating is assigned a letter; “A” for the hard chrome, “E” for the electroless nickel metal, “O” for the hard coat anodized, “H” for the ceramic composite coating, and “B” for the uncoated baseline clutches. Following the letter is the clutch number in each coating set. In the cases that apply, the clutch number is followed by an “M” or “F” for fixed or moveable sheave, respectively. For example, E-2M is the moveable sheave of the second clutch in the electroless nickel metal set.

4.1 Wear Test Stand Results

As outlined in chapter 3 the wear test stand ran each drive clutch for 25 hours. This test time was broken up into three- to seven-hour segments. A new belt was used for each 25 hour test, and belt wear was also recorded. Appendix D – Clutch Run Order, shows the randomized run order, time of each segment, and any comments noted during that segment. During these tests, the rpm of the driven clutch and the hydraulic fluid pressure were recorded. The hydraulic fluid pressure is directly related to the torque applied to the secondary clutch. The wear test stand ran at high load for twenty minutes. At the end of every twenty minutes, the pressure was dropped from approximately 1850 psi, which is a load of 45 ft-lbs of torque, to 450 psi, which is a load of 9 ft-lbs of torque. The pressure remained at 450 psi for four minutes then increased back to 1850 psi, starting a new cycle. During these unloading cycles, the CVT would shift from a low gear to a higher gear then back into a lower gear, and the shift characteristics of the CVT could be observed. This data was then plotted and changes in the shift curves reflected the changes in the shift characteristic. Figure 4-1 gives an example of one of these plots.

As the wear test stand ran at high load, wear grooves developed on the sheaves at a radius near the center of the primary clutch sheaves. By plotting the hydraulic fluid pressure with the rpm of the secondary clutch as a function of time, the amount of delay can be seen between the time the pressure drops and the time the clutch responds. Early in the test the CVT shifted very quickly after a drop in load, shown as noted at A. As the test continued, a delay would develop in shift and in some cases progress until the CVT would not shift at all through an unloading cycle. An example of this delay can be seen at point B noted in Figure 4-1.

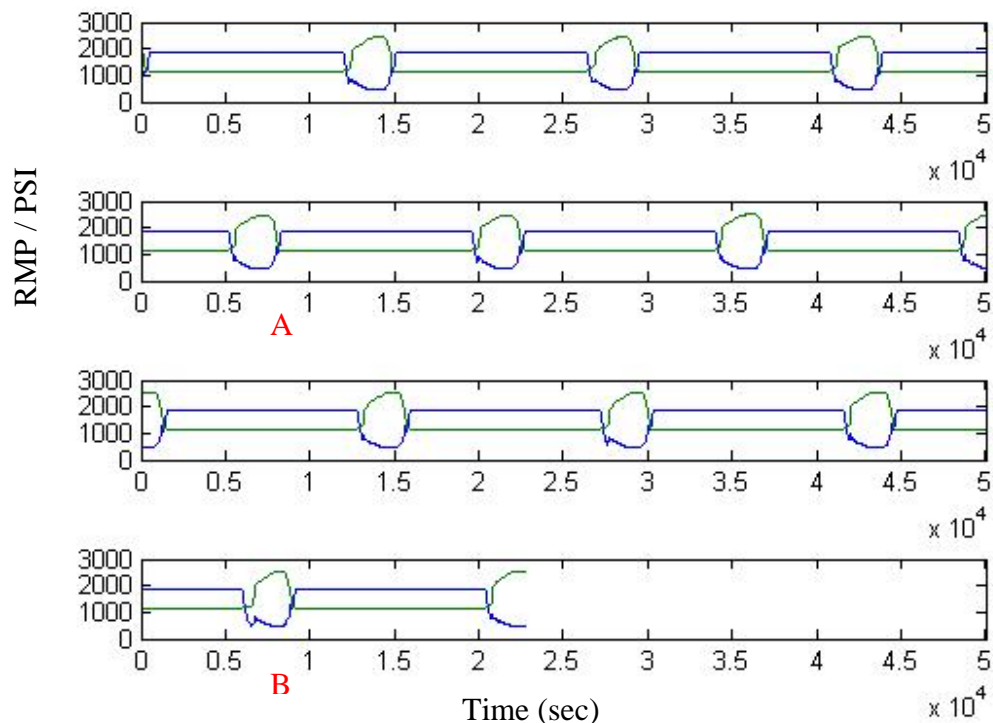


Figure 4-1 Example plot taken from B-2. The blue line is pressure in psi the green line is rpm of the secondary clutch.

The time delay of the shift is a quantifiable factor used to evaluate the performance of the primary clutches. A MATLAB 7.0 program was written to evaluate the shift delay for all of the tests. See appendix E for MATLAB 7.0 m-file.

4.1.1 Shift Characteristics

As discussed above, the shift delay of the tested CVTs was a way to quantify how the primary clutch performed with time. Figure 4-2 shows a comparison of the average shift delay of each coating for the tested drive clutches. Appendix F shows plots of the shift delays for the individual clutches.

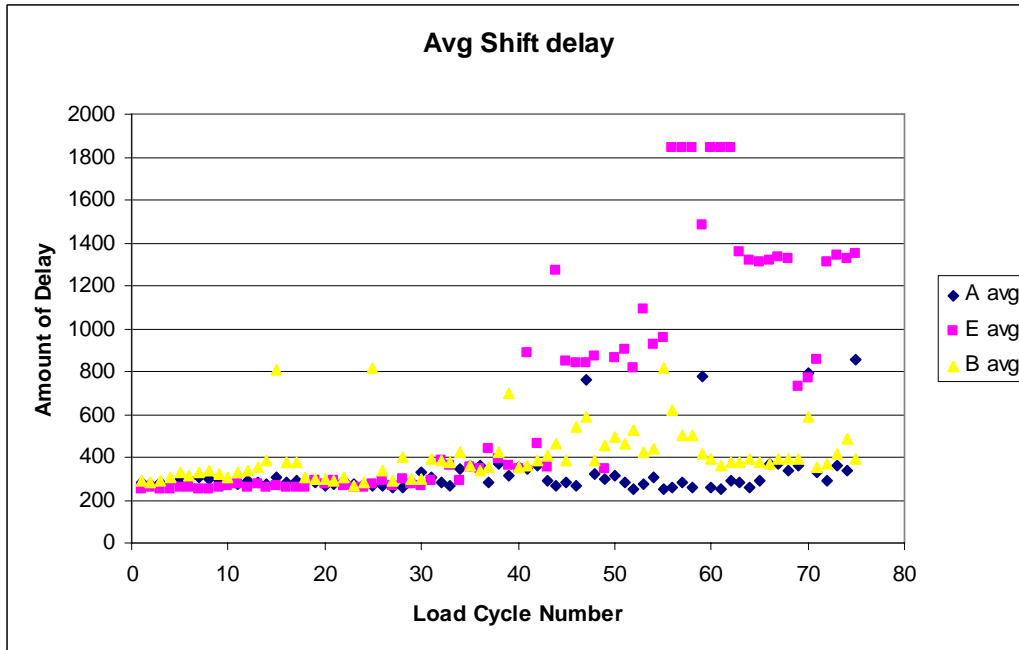


Figure 4-2 Average shift delay of tested primary clutches.

It is important to note that during the first 25 hour test of A-2, it performed extremely poor, see Figure 4-3. Because clutch A-2 missed every shift after the first 12 unloading cycles, additional experiments were conducted to gather more information about this anomaly. The additional tests included running the clutch using the old and a new belt, running with the one-way bearing installed backwards, and with another spring of the same type installed. It was suspected that if installed incorrectly the one-way bearing would affect the CVT performance. The results of these tests did not lead to a clear explanation of why the clutch performed so poorly. It is believed that belt material built up on the outer edge of the lower radius on the primary clutch sheaves created a pseudo wear groove. When this build up was wiped clean during the additional tests, the

clutch returned to normal performance. Based on this observation the data from the second A-2 test was used to create the plot in Figure 4-2 in place of the data from the first test.

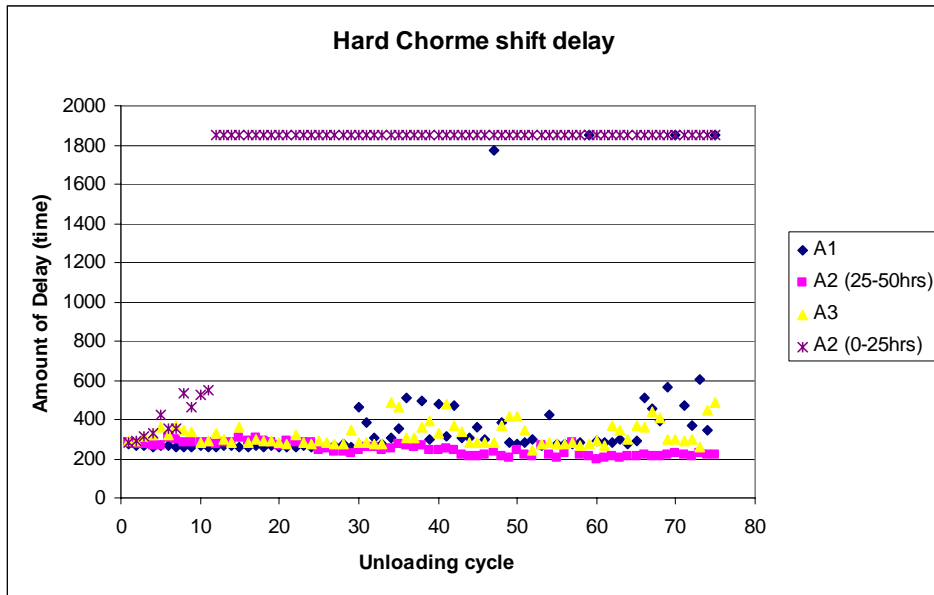


Figure 4-3 Hard chrome shift delay with first 25 hours of A2 test.

4.1.2 Discussion of Shift Delay Results

The electroless nickel coating and the hard chrome coating had lower mean shift delay than the uncoated as unworn clutches, see Table 4-1. The hard chrome coating had a 17% increase in mean shift delay between the first 25 and the last 50 unloading cycles, while the electroless nickel had a 71% increase and the uncoated had a 23% increase for the same periods. For the last 50 unloading cycles, the hard chrome coated clutches had a 22% lower mean shift delay than the uncoated clutches and a 62% lower mean shift delay than the electroless nickel coated clutches.

Table 4-1 Mean shift delay.

Coating	Mean shift Delay		
	Unloading Cycles		
	0-75	0-24	25-75
B	404	339	434
E	693	262	895
A	323	285	341

Based on the shift delay test, the hard chrome coated clutches have the best shift delay performance. Appendix G shows the average shift delay data.

4.1.3 Belt Wear

Belt wear is also a concern in this research. Although coating the CVT sheaves may cause a primary clutch to last longer, if belt wear is excessive then the coating may not be considered a viable option. Likewise, if two coatings have similar wear rates but one causes significantly less belt wear, then this may be the deciding factor of which coating is a better option. Figure 4-4 is a summary of belt wear after 25 hours of CVT testing. In taking the measurements for this wear, it was found that the belts were very inconsistent in width along their length. Because of this inconsistency three measurements were taken at different locations on each belt and the width measurements were averaged. The belt wear shown in Figure 4-4 is the final width minus the average initial width.

The belt wear shown in Figure 4-4 is acceptable because the OEM tolerance on a new belt is plus or minus 0.031 inches and belt wear did not exceed this tolerance. The

table also shows that on average, the belt wear for the hard chrome was 4% greater than for the electroless nickel coated sheaves and the uncoated clutches.

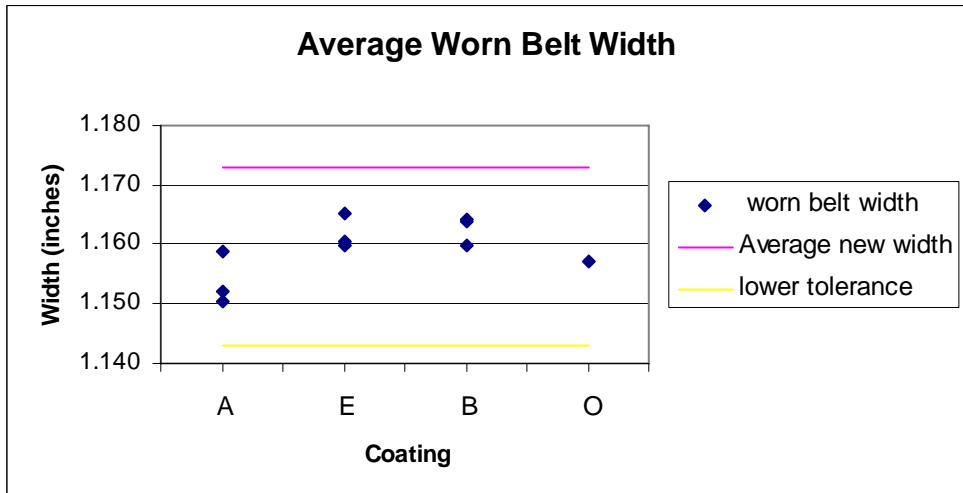


Figure 4-4 Belt width measurements after 25 hours of testing.

4.2 Dynamometer Results

In order to further evaluate the wear of the primary clutch, performance testing was conducted using a 4-wheeler and chassis dynamometer. Acceleration curves for each coated and uncoated clutch were used to evaluate the change in performance.

To compare changes in performance of the clutches each new clutch was tested on the 4-wheeler with the dynamometer before being run on the wear test stand. During this testing, the H (composite ceramic) coatings were eliminated from further testing due to extremely poor dynamometer performance, extreme belt wear, and in one case, coating

delamination. Because of this, the H coatings were not tested on the wear test stand and are not included in any of the results recorded in this chapter.

4.2.1 The Data

As described in chapter 3 the dynamometer software recorded the wheel speed of the ATV. Speed was plotted versus time to yield acceleration curves. Figure 4-5 shows an example of the acceleration curves.

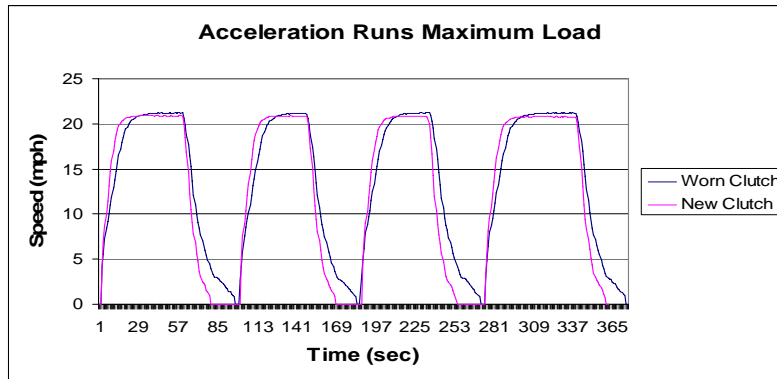


Figure 4-5 Example of formatted acceleration curves.

The slope during acceleration and deceleration was calculated. The slope of the curves gave a single value that could be compared to other runs. Because the slope of the curve near the top was not linear, a percentage of the maximum speed, or the high point of the curve, was used to calculate the slope. The acceleration curves from the dynamometer fit a first order system so the time constant, 62%, of the first order system was used to determine the acceleration slope. Figure 4-6 shows an example of how the acceleration slopes are determined and Table 4-2 shows the calculated values.

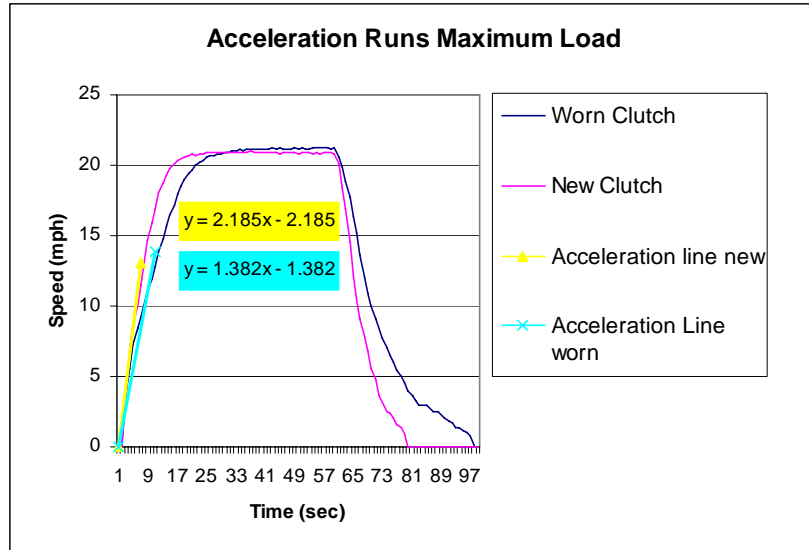


Figure 4-6 Example of acceleration slope.

Table 4-2 Calculated slopes.

Calculated Slopes									
Coating (0 hrs)					Coating (0 hrs)				
		A	B	E		A	B	E	
High	1	20.39707	22.32221	20.7314	1	0.356533	0.313168	0.306252	
	2	20.39461	19.98013	21.55653	2	0.347015	0.345506	0.275526	
	3	19.97635	21.12391	21.47458	3	0.320396	0.306822	0.363783	
Medium	1	20.92245	22.45905	21.11189	1	0.38955	0.396474	0.320258	
	2	20.78578	20.70445	21.88778	2	0.377456	0.3976	0.336341	
	3	20.6467	22.08302	21.75281	3	0.333043	0.344011	0.35327	
Low	1	16.2302	16.4116	16.13146	1	0.294923	0.316647	0.319102	
	2	15.99989	15.83531	16.86686	2	0.305046	0.339033	0.306297	
	3	17.25167	17.14574	16.13004	3	0.328721	0.303718	0.299483	
Coating (25 hrs)					Coating (25 hrs)				
		A	B	E		A	B	E	
High	1	20.46391	22.47849	19.40934	1	0.325345	0.301442	0.322946	
	2	20.38111	21.39219	20.58709	2	0.332523	0.292453	0.314943	
	3	20.92406	21.23909	20.72531	3	0.312589	0.317013	0.344431	
Medium	1	20.69628	23.55517	21.14229	1	0.383895	0.331711	0.335462	
	2	19.6001	21.7409	21.61709	2	0.343345	0.353726	0.346813	
	3	21.31293	24.07121	22.8627	3	0.350095	0.332651	0.335398	
Low	1	16.95831	16.68589	16.94282	1	0.336129	0.288592	0.334035	
	2	17.23565	17.74357	16.85607	2	0.302578	0.332089	0.297562	
	3	17.3976	17.17286	17.87868	3	0.343302	0.308821	0.334817	

4.2.2 The Statistics

With the difference in slope of each acceleration curve calculated, shown in Table 4-3, a statistical analysis could be completed. A two way ANOVA with replications was calculated. The ANOVA was used to determine the effect of coating the clutches and the effect of the loading condition. The two way interaction of the coatings and loading conditions was also investigated using ANOVA. A Bartlett test was run on the variances calculated in the ANOVA to verify that the conditions of the ANOVA test were satisfied. The F test showed the clutch sets did come from their various populations and the ANOVA was applicable. Appendix H shows the details of the analysis. Figure 4-7 shows the effects of the ANOVA

Table 4-3 Change in slope data for Acceleration and Backshift

Acceleration Change in slope Data Effect (0 hrs- 25 hrs)				Backshift Change in Slope Data Effect (0 hrs- 25 hrs)				
Load		A	B	E		A	B	E
High	1	-0.0668	-0.156	1.3221	1	0.0312	0.01173	-0.0167
	2	0.0135	-1.412	0.9694	2	0.0145	0.05305	-0.0394
	3	-0.9477	-0.115	0.7493	3	0.0078	-0.0102	0.01935
Medium	1	0.2262	-1.096	-0.03	1	0.0057	0.06476	-0.0152
	2	1.1857	-1.036	0.2707	2	0.0341	0.04387	-0.0105
	3	-0.6662	-1.988	-1.11	3	-0.0171	0.01136	0.01787
Low	1	-0.7281	-0.274	-0.811	1	-0.0412	0.02806	-0.0149
	2	-1.2358	-1.908	0.0108	2	0.0025	0.00694	0.00874
	3	-0.1459	-0.027	-1.749	3	-0.0146	-0.0051	-0.0353

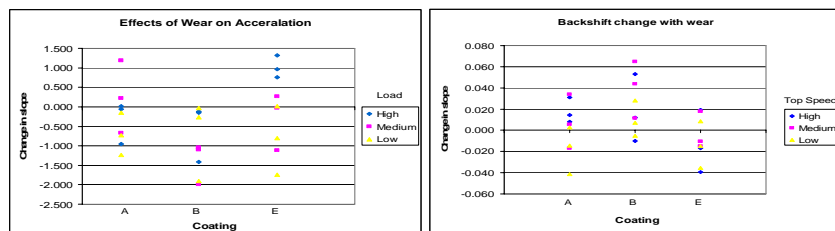


Figure 4-7 Plots showing the change in slope with wear.

The ANOVA test showed that statistically the coated clutches performed better than the uncoated clutches in both the acceleration and backshift tests. Table 4-4 is a summary of the ANOVA. The contrasts were analyzed between the coated and uncoated clutches and between the two coatings seen in Table 4-5. The contrast analysis showed that the coatings were significant but because of high variance there was not enough resolution to tell which of the two coatings was better, although the electroless nickel metal had a larger variance.

Table 4-4 Summary of ANOVA results

Acceleration						
ANOVA						
Source of Variation	SS	df	MS	F	P-value	F critical
Load	2.9723	2.0000	1.4862	2.8473	0.0843	3.5546
Coatings	3.4876	2.0000	1.7438	3.3409	0.0584	3.5546
Interaction	4.9902	4.0000	1.2476	2.3902	0.0891	2.9277
Within	9.3952	18.0000	0.5220			
Total	20.8453	26.0000				
Backshift						
ANOVA						
Source of Variation	SS	df	MS	F _{new}	P _{new}	F
Load	0.00232	2.00000	0.00116	2.23915	0.13027	2.08171
Coatings	0.00479	2.00000	0.00239	4.62763	0.02101	4.30227
Interaction	0.00137	4.00000	0.00034	0.65968		0.61330
Within	0.01002	18.00000	0.00056			
error new	0.01138	22.00000	0.00052			
Total	0.01849	26.00000				

Table 4-5 Summary of contrasts.

Acceleration		Backshift	
Contrasting B with the average of A and E			
C1	1.4760717	C1	-0.05246411
tc1	2.5022876	tc1	-2.82489150
T*	2.1788128	T*	2.17881283
p	0.0277985	p	0.01532027
Contrasting between A and E, B is zero			
C2:	0.2207993	C2:	-0.01210874
Tc2:	0.3743067	Tc2:	-0.65198609
T*	2.1788128	T*	2.17881283
p	0.7147066	p	0.52670131

4.2.3 Discussion of Dynamometer Results

From the dynamometer test it was learned that the coatings have a positive effect on acceleration and backshift characteristics. From this test, the hard chrome coated clutches were chosen as the best performer, because the coating was shown to slow the effect of wear in the acceleration and backshift performance. The hard chrome also had the lower variance between the coated clutches.

4.3 Profilometer Results

The profilometer described in chapter 3 was used to measure the amount of material removed during wear testing. The profilometer would trace the surface of the sheaves creating a radial profile. This profile was then examined for waviness to determine wear groove depth and surface roughness of the worn sheaves.

4.3.1 Surface Waviness of Sheaves

In evaluating the surface waviness and roughness for unworn (new) sheaves, six sheaves had insignificant waviness. Therefore, the assumption was made that all unworn sheaves could be considered to have negligible waviness. All other surface waviness data was taken at 25 hours of wear time. Figure 4-8 is an example of a profile of a worn sheave.

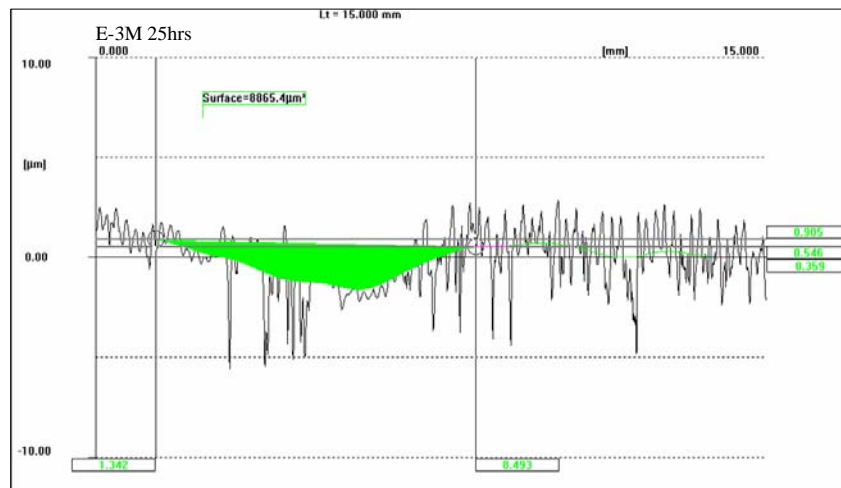


Figure 4-8 Profilometer profile of a moveable sheave after 25 hours of wear.

In Figure 4-8 the black line is the surface roughness profile, the green line is the surface waviness profile, and the green area is the area evaluated as the wear groove. The wear groove areas for both the fixed and movable sheaves were evaluated in this way. Figure 4-9 shows a plot of the fixed, movable, and total sheave cross sectional area. Appendix I shows the actual profile data for all of the sheaves tested.

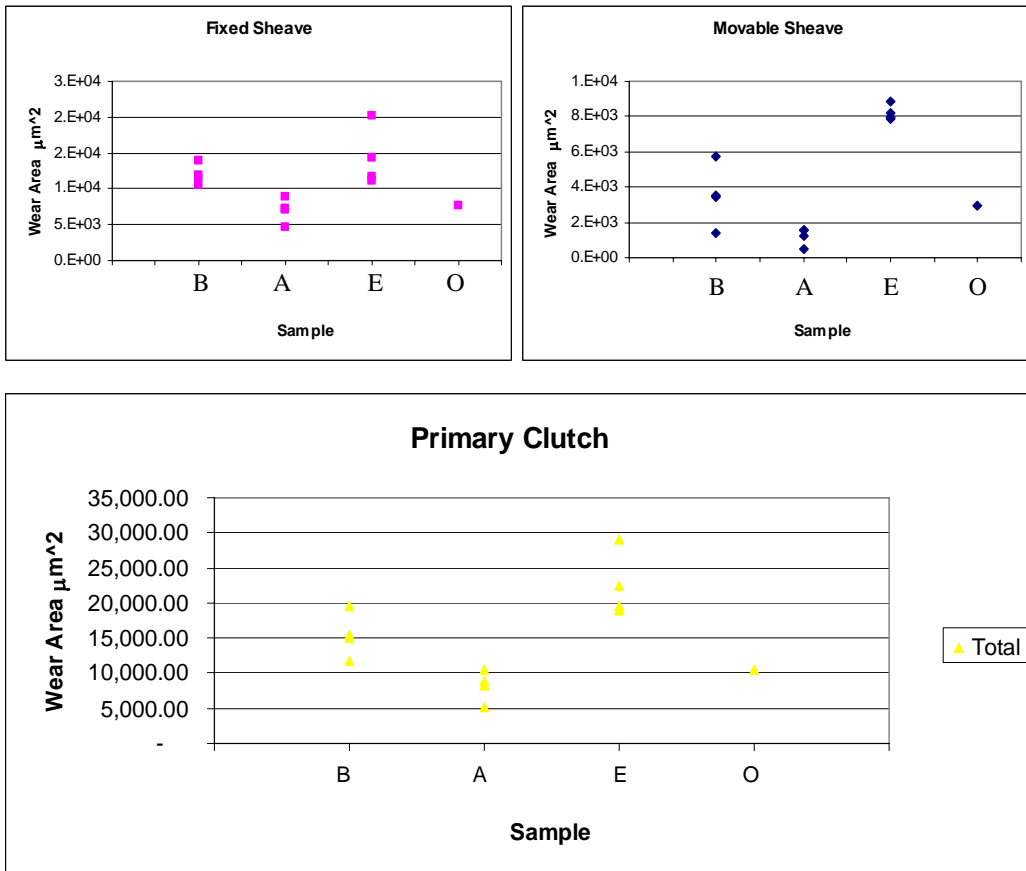


Figure 4-9 Plot showing cross sectional area of wear groove.

From Figure 4-9, it can be seen that the fixed sheave wears more than the movable sheave. Currently, there is no evidence as to the cause of this trend. Another trend was noticed in the wear groove area. Most wear grooves actually exhibited two grooves, one deep groove and one shallow groove with a small peak between the two grooves. Figure 4-10 shows an example of this trend.

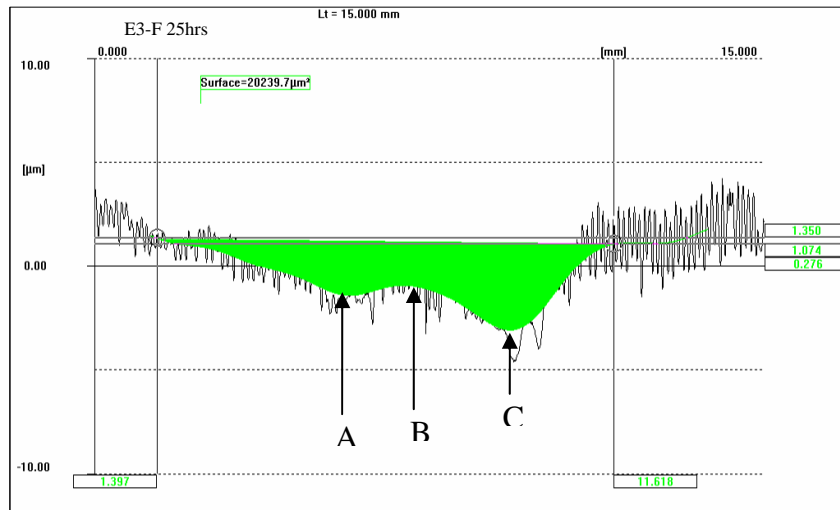


Figure 4-10 Example profile of the two groove trend; where A is the shallow groove, B is the peak, and C is the deep groove.

4.3.2 Surface Roughness of Sheaves

Although surface roughness was not a factor directly considered in the objective of this research, analyzing the data gives evidence of the wear mechanism and helps explain anomalies. Table 4-6 gives the average surface roughness for the unworn coated sheaves as well as the uncoated sheaves. In Table 4-6 Rq is the RMS height, Rt is the largest peak to largest valley distance, Ra is the average distance to the center line, and Rz is the average peak to valley depth.

Table 4-6 Average surface roughness of new clutches.

Surface Roughness Measurement of Unworn Sheaves						
Clutch	B-Fixed	B-Moveable	E-Fixed	E-Moveable	A-Fixed	A-Moveable
Rq (µm)	1.415	1.215	1.15	1.25	1.37	1.59
Rt (µm)	5.48	5.38	5.92	6.1	9.04	9.75
Ra (µm)	1.23	1.06	0.88	1	1.08	1.29
Rz (µm)	5.25	4.635	4.68	5.67	7.2	7.75

As can be seen from Table 4-6, roughest to smoothest sheaves were the hard chrome, uncoated, and electroless nickel. As the sheaves are worn they became smoother as seen in Table 4-7.

Table 4-7 Average of surface roughness measurements taken after 25 hours of testing.

Surface Roughness Measurement of Worn Sheaves						
Clutch	B-Fixed	B-Moveable	E-Fixed	E-Moveable	A-Fixed	A-Moveable
Rq (μm)	0.75	0.91	0.72	1.9	0.87	1.33
Rt (μm)	4.34	5.06	4.94	8.19	6.03	10.26
Ra (μm)	0.60	0.74	0.55	0.86	0.66	1.05
Rz (μm)	3.19	3.81	3.39	7.07	4.87	6.93

4.3.3 Discussion of Profilometer Results

From the figure it can also be seen that hard chrome had the lowest cross sectional wear groove area and the electroless nickel metal coating had the highest. Wear groove cross sectional area, wear groove shape, and wear groove depth were all compared to shift delay of the last five unloading cycles in each clutch. In each case there was some correlation but because of outliers it was concluded that these parameters are not the only significant factor in the performance of the primary clutch. Appendix J shows these plots. This was also supported by the dynamometer tests which showed that the electroless nickel metal clutches performed better than the uncoated clutches even though they had larger wear grooves.

Because the hard chrome coated clutches had the lowest wear groove cross sectional area, it was concluded that the hard chrome coating would effectively lower the wear rate of the primary clutch sheaves.

4.4 Scanning Electron Microscope Results

Three samples for the Scanning Electron Microscope (SEM) were cut from the tested primary clutches. Samples were taken from B-2F, E-3F, and A-2F. The SEM scans of these samples were taken to assist in analyzing the wear scar morphology of the wear grooves and to analyze the chemical makeup of the surface in order to check for foreign particles and possible wear through the coating layer.

4.4.1 Uncoated Aluminum (B-2F) Scans

The scans from the uncoated (base) clutch sheaves did not show very many distinct wear scars or wear morphology. Figure 4-11 shows a scan of a relatively large area of the wear groove. Only one abrasion scar in the radial direction is present. The rest of the area appeared generally smooth.



Figure 4-11 Large area view uncoated wear surface A) Large Si grain B) Radial abrasive scar. Radial direction is vertical.

Using x-ray the darker grains were analyzed for chemical composition. They were found to be mostly silicon. Upon closer investigation and greater magnification (see Figure 4-12 and Figure 4-13) these silicon grains were found to show striations in the direction of wear and show some brittle fracture, labeled A and B in the figure.

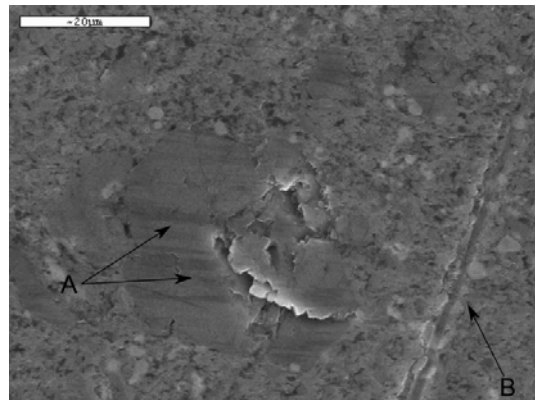


Figure 4-12 Silicon grain with brittle fracture A) Striations in the Si grains, B) Radial wear scar. Radial direction is vertical.

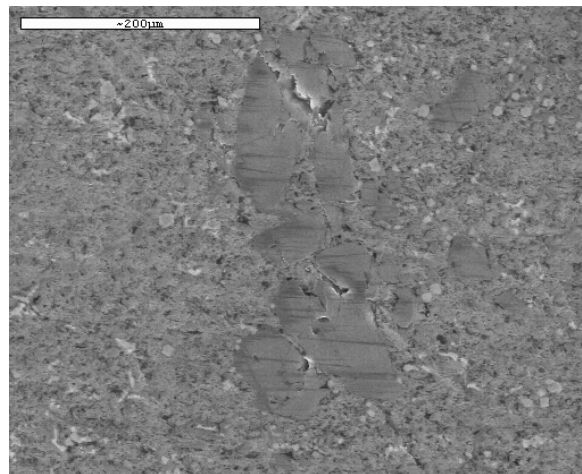


Figure 4-13 Large silicon grain, radial direction is vertical.

The other smaller grains surrounding the large silicon grains are copper and iron grains in the aluminum matrix. From these micrographs mild abrasive wear can be seen on the large silicon grains.

4.4.2 Discussion of Uncoated Scans

Table 4-8 compares the characteristics of adhesive wear with wear characteristics found on the uncoated clutches.

Table 4-8 Comparison of adhesive wear to uncoated clutches

Adhesive wear	
Characteristics - Worn surface can be very smooth - Wear rate are typically low - Surface strength affects wear rates - Softer material can wear a harder - Other material found on surface - Roughness affects wear rates - Cannot be eliminated	Found - SEM scans showed smooth wear surface - Profilometer showed lower wear rate

It was concluded that the dominant wear mechanism for the uncoated clutches was adhesive wear. Although there were wear scars found on the large Si grains they were very shallow and as stated in chapter 3, a softer material can not abrasively wear a harder material, it was concluded that the wear scars found in the Si grain are third-body abrasion. The striations from the abrasive wear can only be seen in the silicon because the silicon grains are much harder than the aluminum; therefore, would have a much lower adhesive wear rate than the aluminum. These conclusions follow the research that

the silicon grains resist wear [18]. It is also believed that adhesive wear is propagating the removal of the silicon particles as they break off of the larger grains these pieces of Si could then become a third-body abrasive.

4.4.3 Electroless Nickel Metal (E-3F) Scans

From the SEM scans of the electroless nickel metal coated sample, it could be seen that, in general, the wear surface was very smooth. The SEM scans distinctly showed two different types of wear scars; pitting and flaking shown in Figure 4-14 and abrasive wear seen at A in Figure 4-15.

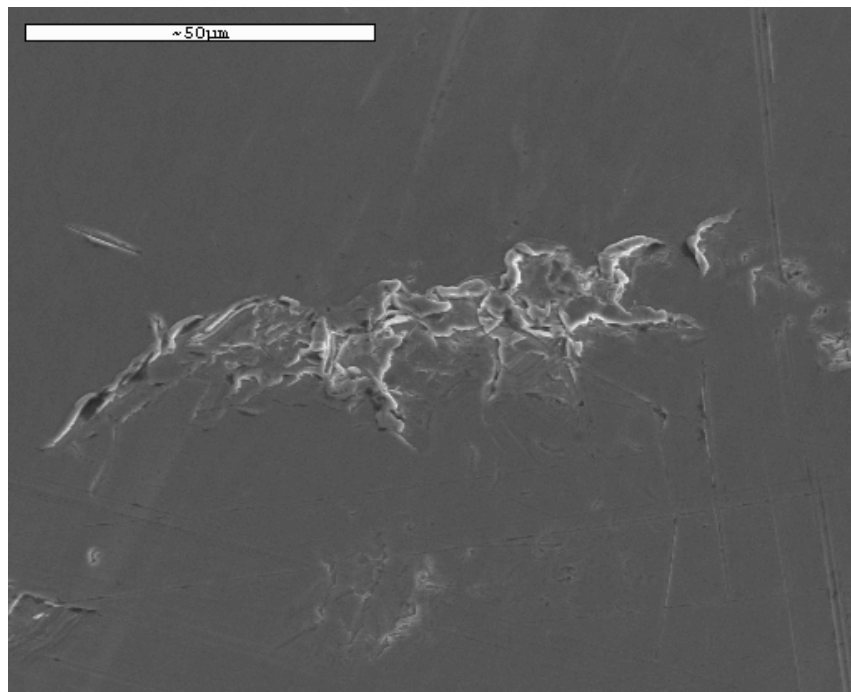


Figure 4-14 Example of surface fatigue. Radial direction is vertical.

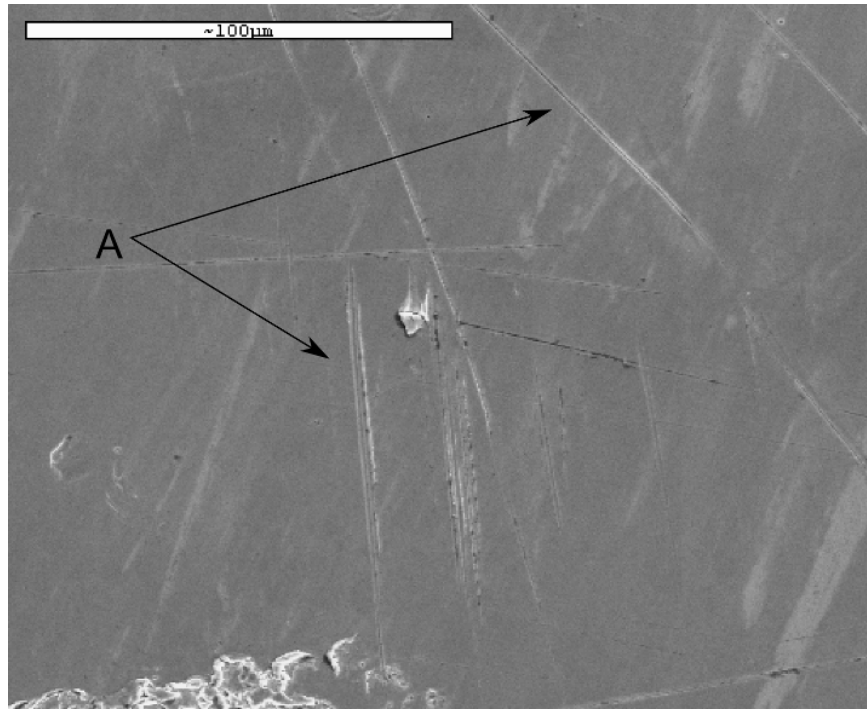


Figure 4-15 Example of abrasion A) radial abrasive wear scars. Radial direction is vertical.

On the electroless nickel SEM sample there were no areas found where the wear had penetrated the coating. The SEM x-ray analysis system has a penetration depth of one micrometer and the aluminum substrate never showed through the coating indicating that the coating is at least one micrometer thick. Note that the original coating thickness was approximately 0.001 inches or 25 micrometers thick. Although the wear never penetrated the coating Figure 4-16 shows possible delimitation of the coating. If wear were to continue this could become a severe problem.

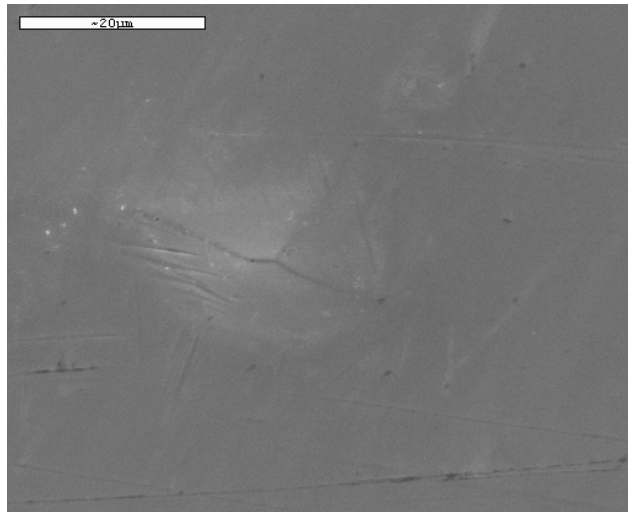


Figure 4-16 Possible delimitation. Radial direction is vertical.

4.4.4 Discussion of Electroless Nickel Scans

Table 4-9 shows the characteristics of surface fatigue wear and the characteristic that were found during testing.

Table 4-9 Wear characteristics compared to fatigue wear

Fatigue Wear	
Characteristics - Pitting and flaking - Incubation period - Wear confined to local stressed area - Sub-surface cracking - High wear rates after incubation - Softer martial can wear a harder	Found - SEM micrographs showed pitting and flaking - Sudden increase in shift delay - Possible incubation period

Surface fatigue wear was determined to be the dominant mechanism of wear. Surface fatigue also correlates with the performance of the electroless nickel metal coating on the wear test stand because an incubation period for crack growth is allowed.

The abrasive wear shown in Figure 4-15 is not very severe and generally in the radial direction. This tells us that abrasion is probably not the dominating mechanism of wear and is mostly occurring during changes in gear ratios. It can also be inferred that there is little tangential slip or there would be more abrasion in the tangential direction and the wear rates would be much higher.

4.4.5 Hard Chrome (A-2F) Scans

The scans from the hard chrome coating were very different from the other SEM scans. The hard chrome surface (see Figure 4-17) is very rough compared to the other coatings even in areas of high wear. The surface also had many holes that seemed relatively deep. As seen in Figure 4-17 and Figure 4-18 the visible effects of wear are apparent where the asperity peaks have been worn. In the areas of high wear, only the valleys have the original surface topology. Also, there were no abrasive scars on the surface.

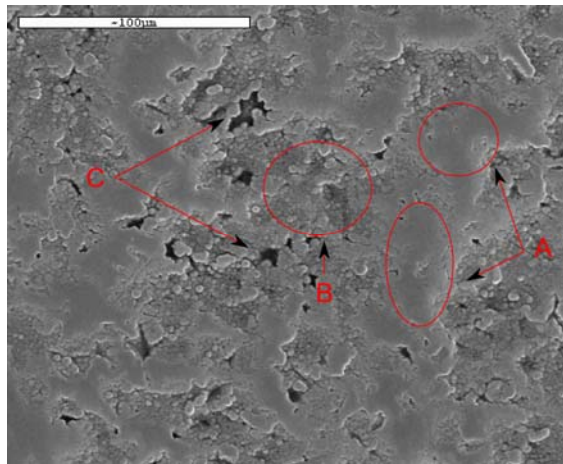


Figure 4-17 Area of high wear A) worn area B) Rough low area C) pits in coating. Radial direction is horizontal.

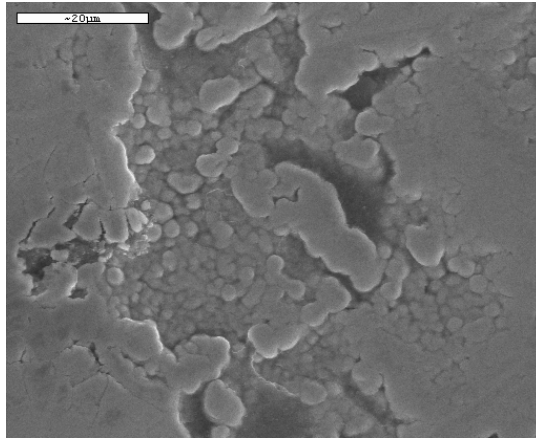


Figure 4-18 No visible abrasive or surface fatigue wear scars. Radial direction is horizontal.

Figure 4-19 shows where a sizeable particle was removed. Although a large particle was removed, only one of these wear scars of was found. Also in this case the particle lost was a piece of the coating as well as a piece of the substrate. The edges of the coating can be seen where coating came off the substrate. It is believed that this particle was a due to a surface defect.

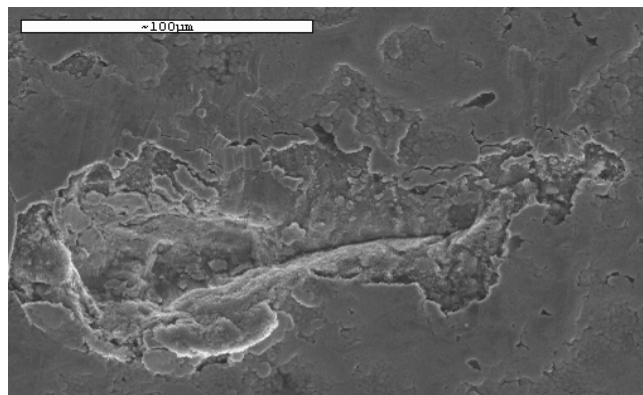


Figure 4-19 Large particle lost due to surface defect. Radial direction is horizontal.

4.4.6 Discussion of Hard Chrome Scans

Table 4-10 compares the characteristics of adhesive wear with characteristic found during testing of the hard chrome coating. Based on Table 4-10 it was determined that the dominant wear mechanism for the hard chrome coating is adhesive wear. Although it was only tested for one sample the wear rate in the hard chrome decreased with time or as the surface became smoother.

Table 4-10 adhesive wear compared with hard chrome.

Adhesive wear	
Characteristics - Worn surface can be very smooth - Wear rate are typically low - Material strength affects wear rates - Softer material can wear a harder - Other material found on surface - Roughness affects wear rates - Cannot be eliminated	Found - SEM scans showed smooth wear surface - Profilometer showed had lowest wear rate - Hard chrome is the hardest surface

Although the uncoated clutches also had adhesive wear as their dominant wear mechanism the hard chrome had a lower wear rate because it is stronger than the die cast aluminum

4.5 Summary of Results

The wear test stand results showed that the hard chrome coating had the lowest average shift delay throughout the 25 hour wear tests. The ANOVA conducted on the dynamometer test results showed that the coatings are significant factors in the change of acceleration and backshift as a result of wear. Also, the hard chrome coating had the

lowest variance. The profilometer test showed that the hard chrome coated clutches had the lowest cross sectional wear groove area. On average, it was 47% less than the uncoated clutches. From the SEM scans of the coated and uncoated wear surfaces, wear scars were seen that indicated the wear mechanisms that are taking place.

5 Conclusions and Future Work

The main conclusion drawn from the data is that the coatings are significant factors in the wear life and performance of the CVT and the hard chrome coating made the most positive impact of the tested coatings. Reasoning for recommending the hard chrome coating as the best candidate to solve the wear problem will be discussed. Finally recommendations for future work will be given.

5.1 Recommendations

Based on the conclusions in section 5.1 and the data in chapter 4 the hard chrome coating is the best candidate tested to solve the wear problem. On average, the hard chrome coating performed the best on the wear test stand, the dynamometer tests, and had the lowest wear rates of all the coated clutches. Although clutch A-2 performed poorly during the first 25 hours of testing this is believed to be due to belt material build on the sheaves and not to wear. In an application where the CVT would shift more frequently this would not be a problem as was shown by the additional testing. The hard chrome had the lowest wear rates and performed well in the dynamometer test. In addition to this, the SEM scans showed that the coating in these test samples never wore through the coating thickness even after a total of 50 hours on the wear test stand.

5.2 Future Work

Although the hard chrome coating performed better than the other coatings, there are still some unknowns regarding this coating. For example, this coating has not been sufficiently tested to determine at what point the wear would wear through the coating material. The performance of the coating in other environments is also unknown. Finally the amount of variation in the coating process is not known.

It is recommended that more samples of hard chrome coating be tested and that the coating be tested in different environments including field testing. This includes ten more samples of the hard chrome coating being run on the wear test stand for a minimum of 50 hours. This testing would give confidence that the coating process and performance would be consistent with the tests already performed. At least two samples should be run until the coating material has been penetrated. This testing would show if there is going to be unexpected wear or performance effects after long use. Finally the coating should be field tested in hot, cold, and dusty conditions. Performing these field tests would indicate if the coating will continue to perform well, even with extreme temperature changes and added abrasives from environmental conditions. Additional testing will also enable better understanding of expected wear rates and the other factors that affect the performance of the CVT such as the surface roughness and the shape of the wear groove.

References

1. Whiting, M.J., *An investigation of improving wear of 390 die-cast aluminum through hardcoat anodizing*. 2005, Brigham Young University. Dept. of Mechanical Engineering, 2005. p. xviii, 104 p.
2. Lansdown, A.R. and A.L. Price, *Materials to resist wear*. 1st ed. 1986, Oxford [Oxfordshire] ; New York: Pergamon Press. ix, 128 p.
3. Bayer, R.G., *Mechanical wear fundamentals and testing*. 2nd ed. 2004, New York: M. Dekker. ix, 399 p.
4. Rabinowicz, E., *Friction and wear of materials*. 1965, New York: Wiley. x, 244 p.
5. Archard, J., *Contact and rubbing of flat surfaces*. J App Phys, 1953. **24**: p. 981-988.
6. Iwabuchi, A., K. Hori, and H. Kudo, *The Effect of Temperature on Wear of S-45-C and Sus-304*. Journal of Japan Society of Lubrication Engineers, 1987. **32**(3): p. 191-197.
7. ASM International., ASM International. Alloy Phase Diagram Committee., and ASM International. Handbook Committee., eds. *ASM handbook*. 1992, ASM International: Materials Park, Ohio. v.
8. Timoshenko, S. and J. Goodier, *Theory of Elasticity*. 1951, New York: McGraw-Hill.
9. Suh, N., *The delamination theory of wear*. Wear, 1973. **25**: p. 111-124.

10. Goldman, R.W., A.E. Segall, and J.C. Conway, *The dry sliding behavior of aluminum alloys against steel in sheave wheel applications*. Journal of Tribology-Transactions of the Asme, 2001. **123**(4): p. 676-681.
11. Kim, Y.S., J.S. Ha, and D.H. Shin, *Sliding wear characteristics of ultrafine-grained non-strain-hardening aluminum-magnesium alloys*. Pricm 5: The Fifth Pacific Rim International Conference on Advanced Materials and Processing, Pts 1-5, 2005. **475-479**: p. 401-404.
12. Strafford, K.N., et al., *Coatings and surface treatment for corrosion and wear resistance*. Ellis Horwood series in applied science and industrial technology. 1984, ChichesterNew York: Published for the Institution of Corrosion Science and Technology by E. Horwood ;Halsted Press. 362 p.
13. Yoshida, M., et al., *Improvement in wear resistance of belt-CVT pulleys by fine particle peening*. Journal of Japanese Society of Tribologists, 2002. **47**(12): p. 901-907.
14. Zhou, F., et al., *Tribological behavior of CrN coating on aluminum alloys deposited by arc ion plating*. Journal of Materials Research, 2002. **17**(12): p. 3133-3138.
15. Nelson, S., *Personal Communication*, D. Mower, Editor. 2006.
16. Chattopadhyay, R., *Surface wear : analysis, treatment, and prevention*. 2001, Materials Park, Ohio: ASM International. xii, 307 p.
17. Sarkar, A.D., *Wear of metals*. 1st ed. 1976, Oxford ; New York: Pergamon Press. xv, 164 p.
18. Elmadagli, M., T. Perry, and A.T. Alpas, *A parametric study of the relationship between microstructure and wear resistance of Al-Si Alloys*. Wear, 2006. **262**(1): p. 79-92.

Appendix A – Hydraulic Fluid Specifications



SHELL TELLUS[®] FLUID HD

Anti-wear synthetic hydraulic fluid

Product Description

Shell Tellus[®] Fluid HD is an anti-wear, hydraulic fluid based on advanced synthetic hydrocarbon technology. Shell Tellus[®] Fluid HD is available in ISO viscosity grade 32. The use of synthetic base fluids with carefully selected additives results in excellent oxidation stability and a wide temperature operating range.

Application

- gear, vane, and piston pumps, particularly those operating over a wide temperature range

Features/Benefits

- excellent oxidation stability
- excellent anti-wear performance
- higher viscosity indexes and lower pour points than mineral oils resulting in performance over a wider temperature range
- good low temperature fluidity
- promotes longer fluid life than petroleum-oil based hydraulic oils

Approvals and Recommendations

- Denison HF-O
- Vickers M-2950-S (Mobile) and I-286-S (Industrial)
- Sundstrand
- Cincinnati Machine

C-M SPECIFICATION	SHELL PRODUCT
P-68	Tellus Fluid HD 32

Typical Properties of Shell Tellus® Fluid HD

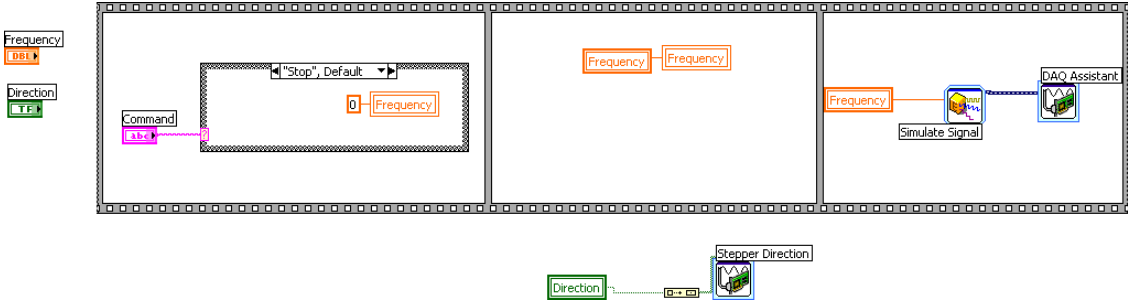
	Test Method	ISO Viscosity Grade
		32
Product Code		65475
Specific Gravity, 15.6°C	D1298	0.829
Density, Lb/Gal, 15.6°C		6.93
Viscosity:		
@ 40°C, cSt	D445	30.4
@ 100°C, cSt	D445	5.8
Viscosity Index	D2270	136
Flash Point, COC, °C	D92	230
Pour Point, °C	D97	<-54
Fire Point, COC, °C	D92	266
Rust Protection, ASTM		
	D665A	Pass
	D665B	Pass
Foam Seq. I	D892	Trace
Seq. II	D892	Trace
Seq. III	D892	Trace
Emulsion, vol @ 130°F (minutes)	D1401	40/40/0 (15)
Air Release, 50°C, minutes	DIN 51381	1
PNEUROP Oxidation, % residue	DIN 51352	0.1
Vapor Pressure, mm Hg	Isoteniscope	
@ 300°F		0.7
@ 400°F		3.8
@ 450°F		7.2
Specific Heat, Cp, CAL/g- °C	D2766	
37.8°C (100°F)		0.52
93.0°C (200°F)		0.57
Thermal Conductivity, Heat Probe Method BTU/HR - FT - [°F / Ft]	Heat Probe	
37.8°C (100°F)		0.089
93.0°C (200°F)		0.087
FZG Gear Test, stage	DIN 51354	11

Appendix B – Labview Block Diagram

5.3 Clutch_Testing_Program.vi



5.6 Motor_On_Time.vi



Appendix C – Hommel Tester T8000 Specifications



HOMMEL TESTER T8000 – Technical specifications Roughness measurement

PC evaluation unit	Evaluation unit, monitor, printer, keyboard, mouse, including measuring electronics for data logging and control of peripherals
Measuring method	Skidless/skid measurement, calibrated
Accuracy according to DIN 4772	Class 1
Measuring ranges/Resolution	± 8 µm / 1 nm ± 80 µm / 10 nm ± 800 µm / 100 nm ± 8000 µm / 1000 nm
Metric system	µm/inch selectable
Filter	
Cut-offs	0.025 / 0.08 / 0.25 / 0.8 / 2.5 / 8.0 (mm) selectable -2 to +1 cut-off steps individual 0.001 to 80 in 0.001 increments
DIN 4768	RC, digitally calculated (mm) Cut-offs 0.025 / 0.08 / 0.25 / 0.8 / 2.5 / 8.0
DIN EN ISO 11562, Part 1 (50% Gauss)	Gauss (M1) Digital filter (mm) Cut-offs 0.025 / 0.08 / 0.25 / 0.8 / 2.5 / 8.0
DIN EN ISO 13565-1	2-fold Gauss (M2) Rk parameters Cut-offs 0.025 / 0.08 / 0.25 / 0.8 / 2.5 / 8.0
ISO 3274/11562	Short-wave cut-offs λs, individual λc/λs 30 / 100 / 300
ISO 3274/11562	Form filter λf
Tracing speed Vt	It – 0.05 / 0.15 / 0.5 mm/s or variable 0.01-2.0 mm/s in 0.01 increments
Tracing length It	0.48 / 1.5 / 4.8 / 15 / 48 mm or variable 0.1-200 mm
Measuring length lm	0.40 / 1.25 / 4.0 / 12.5 / 40 mm or variable
Cut-off λ (mm)	0.08 / 0.25 / 0.8 / 2.5 / 8.0
Roughness parameters DIN EN ISO 4287	Ra; Rz; Rmax; Rt; Rq; Rsk; lmo; lo; Rdq; da; ln; La; Lq; Rz-ISO; R3z; Rpm; Rp3z; R3zm; Rp; D; RPl; RSm; Rpm/R3z; lr; Rku; tpi; tpi; tpi; Rt/Ra; Rz1; Rz2; Rz3; Rz4; Rz5; Rmr; Rmr%; Api
Rk parameters DIN EN ISO 13565	Rpk*; Rpk; Rk; Rvk; Rvk*; Mr1; Mr2; A1; A2; Vo(70%)0.01*; Rv/Rk
Profile parameters DIN EN ISO 4287	Pt; Pz; Pz; Pa; Pq; Psk; PSm; Pdq; lp; Pku; tpa; tpa; tpa; tpa; Pmr0; Apa; Apa%; Pmr; Pmr%
Waviness parameters DIN EN ISO 4287	Wt; Wp; Wz; Wa; Wq; Wsk; WSm; Wdq; lw; Wku; WD1t; WWD1z; WD1a; WD1q; WD1Sm; WD1dq; WD1lw; WD1Pc; WD2t; WD2p; WD2z; WD2a; WD2q; WD2sk; WD2Sm; WD2dq; WD2lw; WD2ku; WD2Pc
Motif parameters DIN EN ISO 12085	R; Rx; AR; Nr; W; Wx; AW; Nw; Wte; Tpa (CR, CL, CF)
Roughness parameters JIS B-0601	Rz-JIS; Rmax-JIS
Statistics	(n, x, S, R, max, min) 1 - 999 measurements
Screen and printout forms	User defined: surface parameters, statistics, profile position, P-/ R-/ W-/ K-profile, material ratio, measuring conditions, tolerances, topography (optional)
Operational modes	Programme creation, CNC-run (optional), measurement with pre-selected programmes, automatic measuring run, profile measurement, profile analysis, adjustment
Alignment	Profile inversion, coarse alignment, fine alignment, partial alignment
Peripheral equipment	Traverse units: waveline™ 20/60/120/200, LV50-LV250, RV150S Rotary traverse units: waverotor™, RV 150 S Measuring columns: wavelift™ 400/CNC, 800/CNC Tilting units: wavelift™ 60/120/200 Contour pick-ups: wavecontour™ inductive/digital Topography: Y positioner
Languages	German, English, French, Italian, Spanish, Czech
General data	
Power supply	100V-120V / 200V-240V selectable, 50-60 Hz, 400 VA
Operating temperature	-5°C to +40°C, relative humidity max. 85% without condensation
Storage temperature	-20°C to +50°C

Subject to change without notice. 06/03

Hommelwerke GmbH,
Alte Tuttlinger Straße 20,
D-78056 VS-Schwenningen
Phone +49(0)77 20/6 02-0,
Fax +49(0)77 20/6 02-1 23,
E-Mail: info@hommelwerke.de

Appendix D – Clutch Run Order

D- 1 Run Order

Primary Clutch Run Order		
Clutch	time (total)	Comments
B-2	3 (3)	
B-2	3 (6)	
B-2	4 (10)	
B-2	15 (25)	CVT started making very loud pitched squealing noise. Additional belt slip is suspected
O-1	4 (4)	
O-1	3 (7)	CVT started making very loud pitched squealing noise. Additional belt slip is suspected
O-1	4 (11)	
O-1	1.66 (12.66)	
O-1	2.33 (15)	
A-1	4.66 (4.66)	
A-1	7.33 (12)	CVT started making very loud pitched squealing noise. Additional belt slip is suspected
A-1	4 (16)	
A-1	4 (20)	
A-1	5 (25)	
O-1	5 (20)	extreme belt noise continued
O-1	5 (25)	
E-3	6 (6)	
E-3	5 (11)	small amount of belt build-up at larger diameter valve was opened all the way to clean
E-3	5 (16)	no build up this time
E-3	6 (22)	
E-3	3 (25)	there was never any extreme belt
A-2	5 (5)	
A-2	7 (12)	extreme belt noise started
A-2	6 (18)	
A-2	5 (23)	
E-1	7 (7)	
E-1	6 (13)	
E-1	4 (17)	
E-1	6 (23)	
E-1	2 (23)	there was never any extreme belt noise
A-2	2 (25)	
A-3	3 (3)	
A-3	7 (10)	extreme belt noise
A-3	5 (15)	extreme belt noise became sporadic
A-3	5 (20)	

D- 2 continued

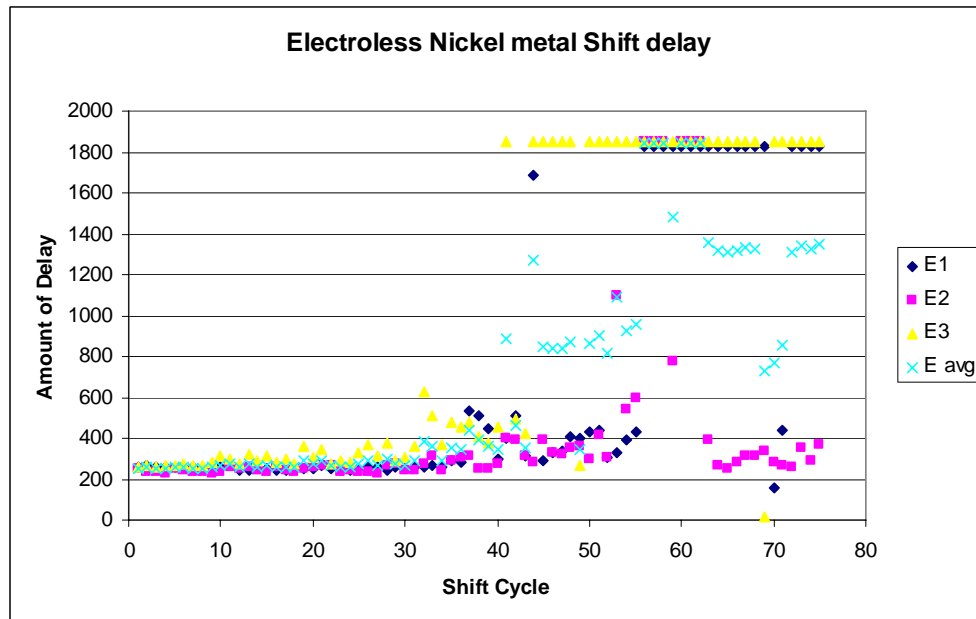
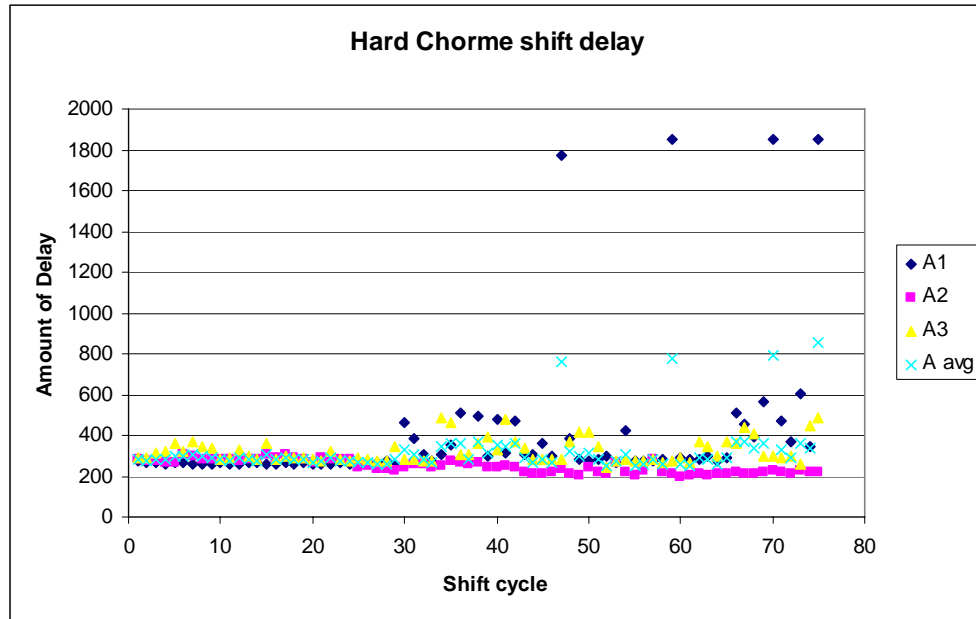
A-3	5 (25)	
E-2	5 (12)	
E-2	7 (19)	
E-2	6 (25)	
A-2	4.5 (4.5)	Additional wear test
A-2	1 (5.5)	Additional wear test
A-2	1 (6.5)	Additional wear test
A-2	.5 (7)	Additional wear test
A-2	7 (14)	Additional wear test
A-2	7 (21)	Additional wear test
A-2	4 (21)	Additional wear test
B-1	7 (7)	Before Clutches was run sheaves had a very porous surface
B-1	7 (14)	
B-1	7 (21)	
B-1	4 (25)	
B-3	7 (7)	
B-3	7 (14)	
B-3	5 (19)	
B-3	6 (25)	

Appendix E – MATLAB 7.0 m-file code

```
x = 1;
num = 1;
clear t;
while data(x,1) > -1;
    y = 1;
    if data(x,2) - data(x+15,2) > 70
        while data(x,5) < 1275 & y < 1850
            y = y + 1;
            x = x + 1;
        end
        if y > 2
            t(num,1) = num;
            t(num,2) = y;
            t1(num,1) = y;
            num = num + 1;
            x = x - 1;
        end
    end
    x = x + 1;
end
t
figure;
plot(t, '.')

axis([0 75 200 1900 ]);
```


Appendix F – Shift delay plots



Appendix G – Statistics for shift delay

A avg	E avg	B avg	A avg		E avg		B avg	
281	255	287						
276	257	280	Mean	323	Mean	693	Mean	404
285	253	293	Standard Error	14	Standard Error	61	Standard Error	14
284	250	307	Median	287	Median	358	Median	380
297	259	330	Mode	280	Mode	1842	Mode	380
297	259	316	Standard Deviation	118	Standard Deviation	525	Standard Deviation	119
307	254	328	Sample Variance	13939	Sample Variance	275589	Sample Variance	14109
296	252	341	Kurtosis	13	Kurtosis	0	Kurtosis	4
293	255	320	Skewness	4	Skewness	1	Skewness	2
279	267	309	Range	603	Range	1592	Range	547
278	272	330	Minimum	250	Minimum	250	Minimum	270
288	257	337	Maximum	853	Maximum	1842	Maximum	816
280	275	351	Sum	24227	Sum	51943	Sum	30265
276	261	383	Count	75	Count	75	Count	75
308	265	808						
280	261	374						
291	262	380						
282	256	303						
279	288	301						
270	272	295						
273	291	293						

287	263	307	<i>A avg</i>			<i>E avg</i>			<i>B avg</i>		
277	256	270									
275	256	280	Mean	284.9722	Mean	262.3333	Mean	338.5			
268	272	816	Standard Error	2.086969	Standard Error	2.173716	Standard Error	21.38486379			
267	288	334	Median	281.3333	Median	259	Median	312.5			
260	266	292	Mode	279.6667	Mode	257	Mode	293.3333333			
262	297	397	Standard Deviation	10.22402	Standard Deviation	10.64899	Standard Deviation	104.764009			
279	274	301	Sample Variance	104.5306	Sample Variance	113.401	Sample Variance	10975.49758			
328	265	300	Kurtosis	0.054024	Kurtosis	2.111452	Kurtosis	19.37844916			
310	288	389	Skewness	0.877205	Skewness	1.546701	Skewness	4.222716361			
280	387	382	Range	37.33333	Range	41.33333	Range	538.3333333			
264	362	380	Minimum	270.3333	Minimum	250	Minimum	269.6666667			
346	289	427	Maximum	307.6667	Maximum	291.3333	Maximum	808			
364	353	361	Sum	6839.333	Sum	6296	Sum	8124			
360	347	339	Count	24	Count	24	Count	24			
280	441	350									
372	390	422									
312	358	701	<i>A avg</i>			<i>E avg</i>			<i>B avg</i>		
349	343	349									
347	885	358	Mean	340.9281	Mean	895.0458	Mean	434.130719			
360	466	384	Standard Error	19.58362	Standard Error	73.71834	Standard Error	15.87152141			
288	350	408	Median	293.3333	Median	853.3333	Median	394.3333333			
267	1272	462	Mode	268	Mode	1841.667	Mode	380.3333333			
284	845	387	Standard Deviation	139.855	Standard Deviation	526.4543	Standard Deviation	113.3453342			
268	838	542	Sample Variance	19559.42	Sample Variance	277154.1	Sample Variance	12847.16479			
762	836	590	Kurtosis	7.393998	Kurtosis	-1.049874	Kurtosis	3.851243926			
322	868	383	Skewness	2.857592	Skewness	0.391025	Skewness	1.887507529			
302	343	454	Range	603	Range	1576.333	Range	524.6666667			
313	859	496	Minimum	250	Minimum	265.3333	Minimum	291.6666667			
282	901	462	Maximum	853	Maximum	1841.667	Maximum	816.3333333			
250	819	529	Sum	17387.33	Sum	45647.33	Sum	22140.66667			
271	1094	424	Count	51	Count	51	Count	51			
309	929	442									
252	959	814									
262	1842	623									
280	1842	498									
256	1842	504									
779	1485	413									
260	1842	394									
250	1842	361									
287	1842	374									
283	1357	380									
261	1314	395									
291	1308	374									
365	1320	367									

Appendix H – ANOVA and MATLAB 7.0 code

Anova: Two-Factor With Repl

Analysis of Forward Shift

SUMMARY	Hard chrone	Uncoated	Electroless	Total	Bartlet Test	
<i>Max Load</i>						
Count	3	3	3	9		
Sum	-1.001047	-1.68352	3.040775	0.356208		
Average	-0.333682	-0.561173	1.013592	0.039579		
Variance	0.284383	0.543428	0.083485	0.771172	P-value	0.497
					chi square	1.39658
<i>Medium Load</i>						
Count	3	3	3	9		
Sum	0.74562	-4.120765	-0.8696	-4.244745		
Average	0.24854	-1.373588	-0.289867	-0.471638		
Variance	0.857771	0.284195	0.526988	0.929193	P-value	0.768
					Chi square	0.52712
<i>Low Load</i>						
Count	3	3	3	9		
Sum	-2.109805	-2.209672	-2.549212	-6.868689		
Average	-0.703268	-0.736557	-0.849737	-0.763188		
Variance	0.297393	1.044939	0.774997	0.533754	P-value	0.711
					chi square	0.68088
<i>Total</i>						
Count	9	9	9	27		
Sum	-2.365231	-8.013957	-0.378037	-10.75723		
Average	-0.262803	-0.89044	-0.042004	-0.398416		
Variance	0.532576	0.605214	1.031924	0.801742		
<i>ANOVA</i>						
Source of Variation	SS	df	MS	F	P-value	F critical
Load	2.9723	2.0000	1.4862	2.8473	0.0843	3.5546
Coatings	3.4876	2.0000	1.7438	3.3409	0.0584	3.5546
Interaction	4.9902	4.0000	1.2476	2.3902	0.0891	2.9277
Within	9.3952	18.0000	0.5220			
Total	20.8453	26.0000				

Anova: Two-Factor With Replication Analysis of Back Shift

SUMMARY	Hard Chroi	Uncoated	Electroless	Total	
High Load					
Count	3	3	3	9	
Sum	0.053486	0.054589	-0.036759	0.071316	
Average	0.017829	0.018196	-0.012253	0.007924	Chisquare 1.60967
Variance	0.000145	0.001031	0.000878	0.000743	P-value 0.447
Medium Load					
Count	3	3	3	9	
Sum	0.022715	0.119997	-0.007804	0.134907	
Average	0.007572	0.039999	-0.002601	0.01499	Chisquare 0.32482
Variance	0.000657	0.000724	0.00032	0.000797	P-value .85
Low Load					
Count	3	3	3	9	
Sum	-0.053319	0.029896	-0.041533	-0.064956	
Average	-0.017773	0.009965	-0.013844	-0.007217	Chisquare 0.16577
Variance	0.000484	0.000282	0.000486	0.000482	P-value 0.92
Total					
Count	9	9	9	27	
Sum	0.022882	0.204481	-0.086096	0.141267	
Average	0.002542	0.02272	-0.009566	0.005232	
Variance	0.000574	0.00069	0.000449	0.000711	

ANOVA	SS	df	MS	Fnew	Pnew	F
Source of Variation						
Load	0.00232	2.00000	0.00116	2.23915	0.13027	2.08171
Coatings	0.00479	2.00000	0.00239	4.62763	0.02101	4.30227
Interaction	0.00137	4.00000	0.00034	0.65968		0.61330
Within	0.01002	18.00000	0.00056			
error new	0.01138	22.00000	0.00052			
Total	0.01849	26.00000				

Matlab Code for acceleration curves analysis

```
//Load in File name
clear
clc
per_speed = .625
Filename='B3max.csv'

cd /home/peter/Desktop/4-wheeler/dyno_testing/25_hrs_nov-28/Formatted_Data/
//cd /home/peter/Desktop/4-wheeler/dyno_testing/NEW_nov-15/Formatted_data
```

```

x=read(Filename,-1,2);
max_speed=max(x(:,2))
//let's find where the four runs are located at
loc_run=find(x(:,2)==0);

//lets find the time values of % of the max speed

loc_run_last=0;

t=find(x(loc_run(1):loc_run(2),2)>= per_speed*max_speed);
time_1=x(loc_run(1),1);
time_2=x((t(1)+loc_run_last),1);
time_3=x((t(1)+loc_run_last-1),1);
speed_2=x((t(1)+loc_run_last),2);
speed_3=x((t(1)+loc_run_last-1),2);
interp_x= time_3+(max_speed*per_speed-speed_3)*(time_2-
time_3)/(speed_2-speed_3);
acl(1)=max_speed*per_speed/(interp_x-time_1);
loc_run_last=loc_run(2);

t=find(x(loc_run(3):loc_run(4),2)>= per_speed*max_speed);
time_1=x(loc_run(3),1);
time_2=x((t(1)+loc_run_last),1);
time_3=x((t(1)+loc_run_last-1),1);
speed_2=x((t(1)+loc_run_last),2);
speed_3=x((t(1)+loc_run_last-1),2);
interp_x= time_3+(max_speed*per_speed-speed_3)*(time_2-
time_3)/(speed_2-speed_3);
acl(2)=max_speed*per_speed/(interp_x-time_1);
loc_run_last=loc_run(4);

t=find(x(loc_run(5):loc_run(6),2)>= per_speed*max_speed);
time_1=x(loc_run(5),1);
time_2=x((t(1)+loc_run_last),1);
time_3=x((t(1)+loc_run_last-1),1);
speed_2=x((t(1)+loc_run_last),2);
speed_3=x((t(1)+loc_run_last-1),2);
interp_x= time_3+(max_speed*per_speed-speed_3)*(time_2-
time_3)/(speed_2-speed_3);
acl(3)=max_speed*per_speed/(interp_x-time_1);
loc_run_last=loc_run(6);

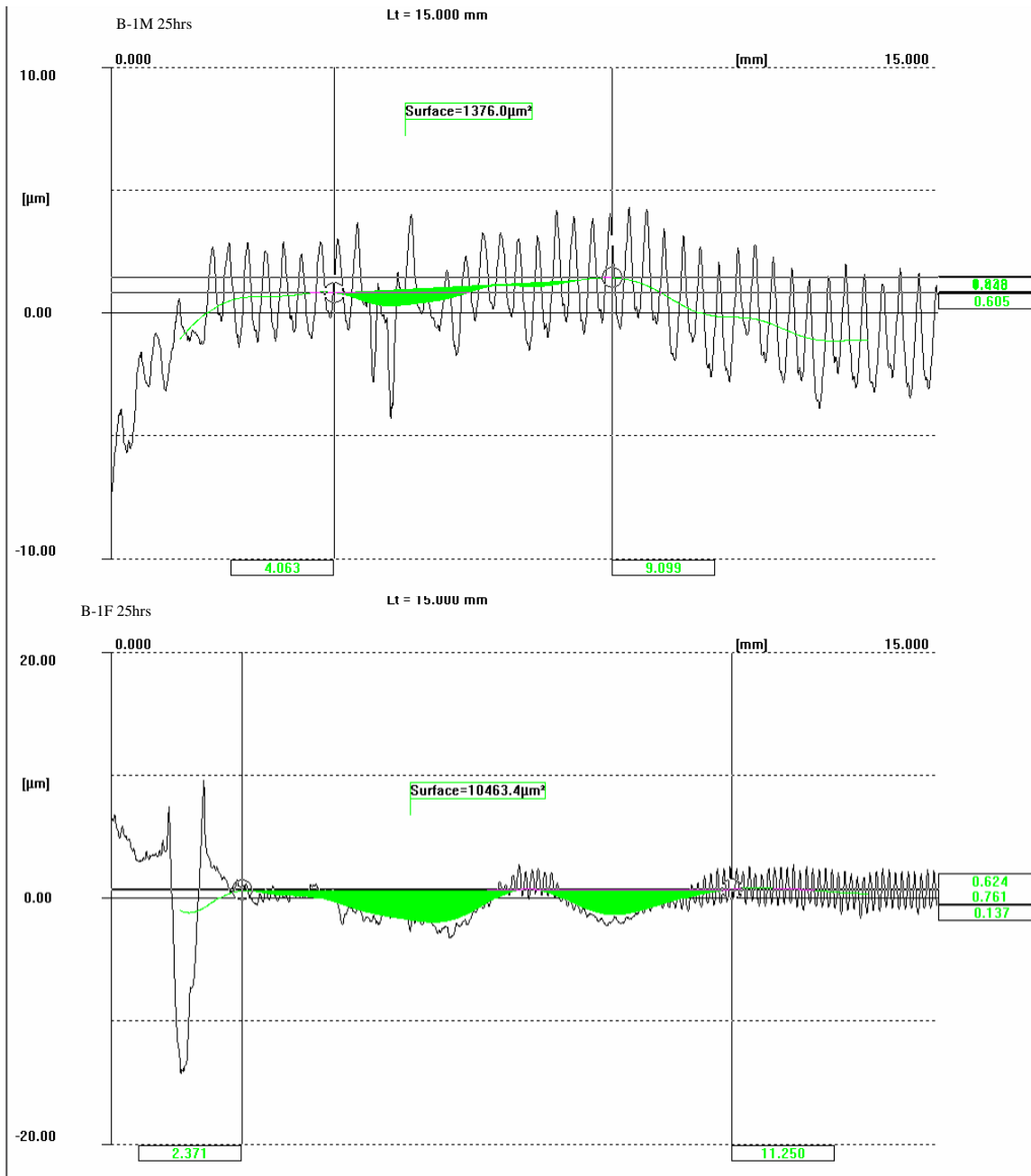
t=find(x(loc_run(7):loc_run(8),2)>= per_speed*max_speed);
time_1=x(loc_run(7),1);
time_2=x((t(1)+loc_run_last),1);
time_3=x((t(1)+loc_run_last-1),1);
speed_2=x((t(1)+loc_run_last),2);
speed_3=x((t(1)+loc_run_last-1),2);
interp_x= time_3+(max_speed*per_speed-speed_3)*(time_2-
time_3)/(speed_2-speed_3);
acl(4)=max_speed*per_speed/(interp_x-time_1);
acl

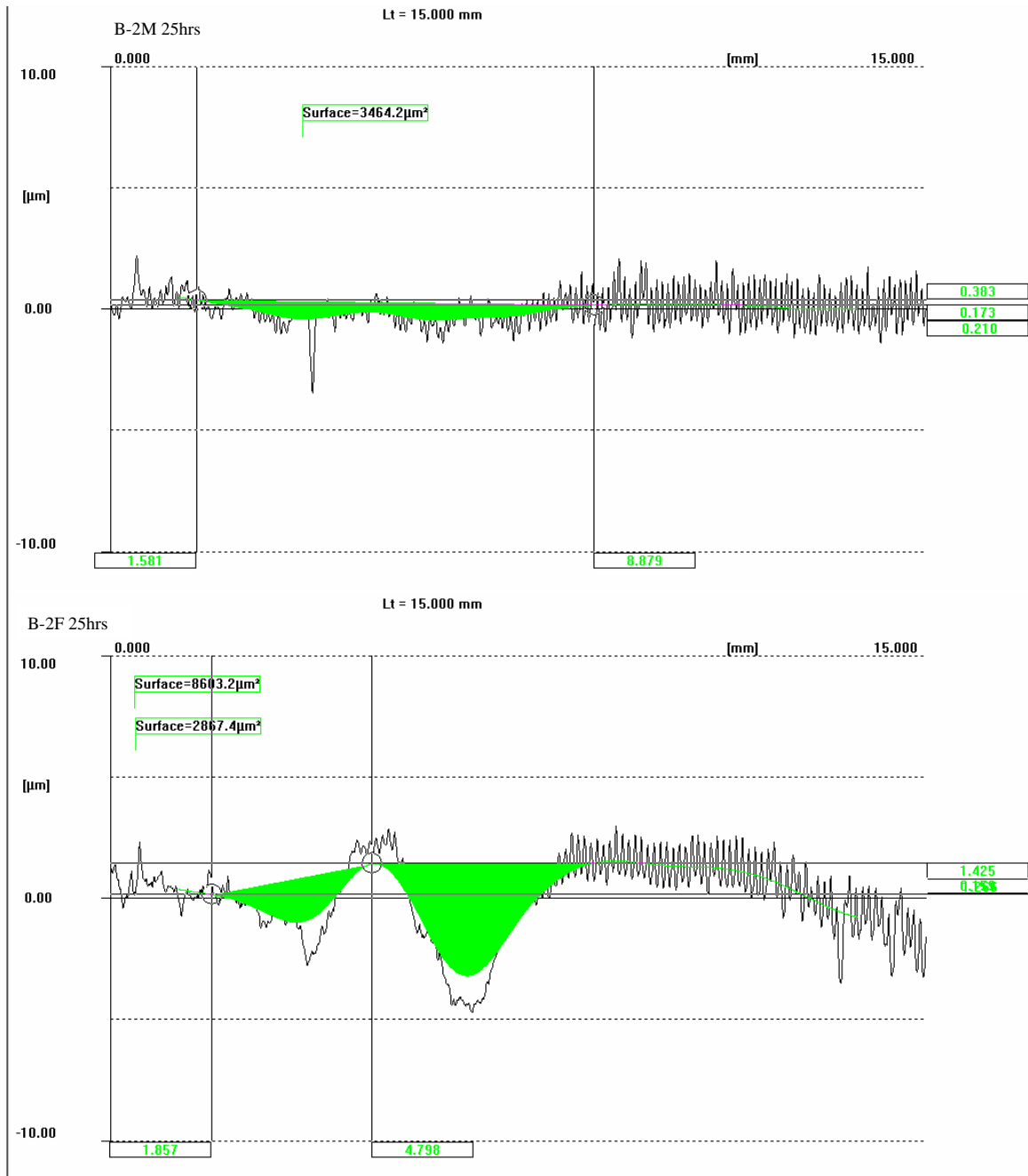
//lets plot these one on top of the other

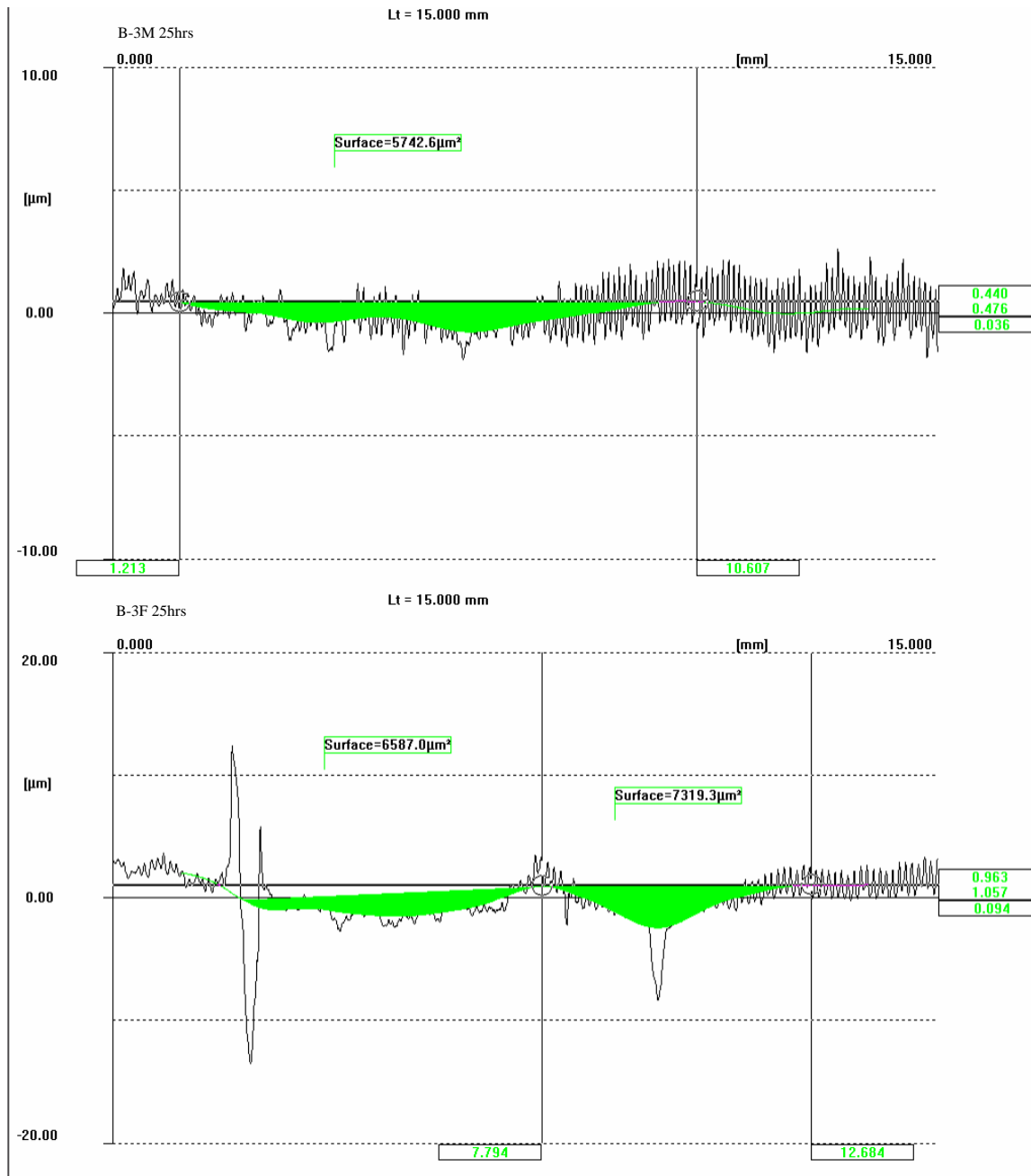
```

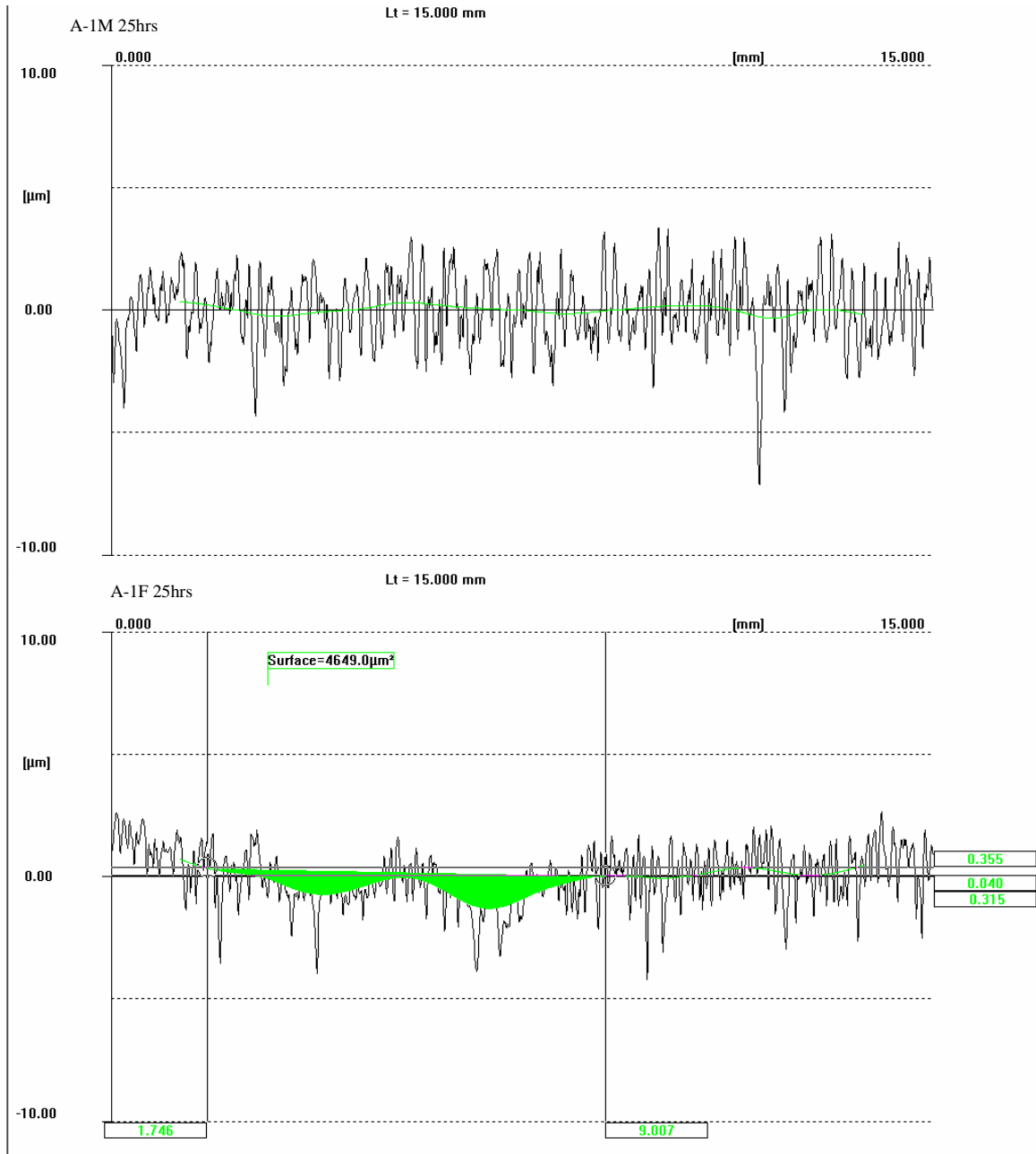
```
    plot(x(loc_run(1):loc_run(2),1)-
x(loc_run(1),1),x(loc_run(1):loc_run(2),2))
    plot(x(loc_run(3):loc_run(4),1)-
x(loc_run(3),1),x(loc_run(3):loc_run(4),2))
    plot(x(loc_run(5):loc_run(6),1)-
x(loc_run(5),1),x(loc_run(5):loc_run(6),2))
    plot(x(loc_run(7):loc_run(8),1)-
x(loc_run(7),1),x(loc_run(7):loc_run(8),2))
    plot(x(loc_run(7):loc_run(8),1)-x(loc_run(7),1),per_speed*max_speed)
```

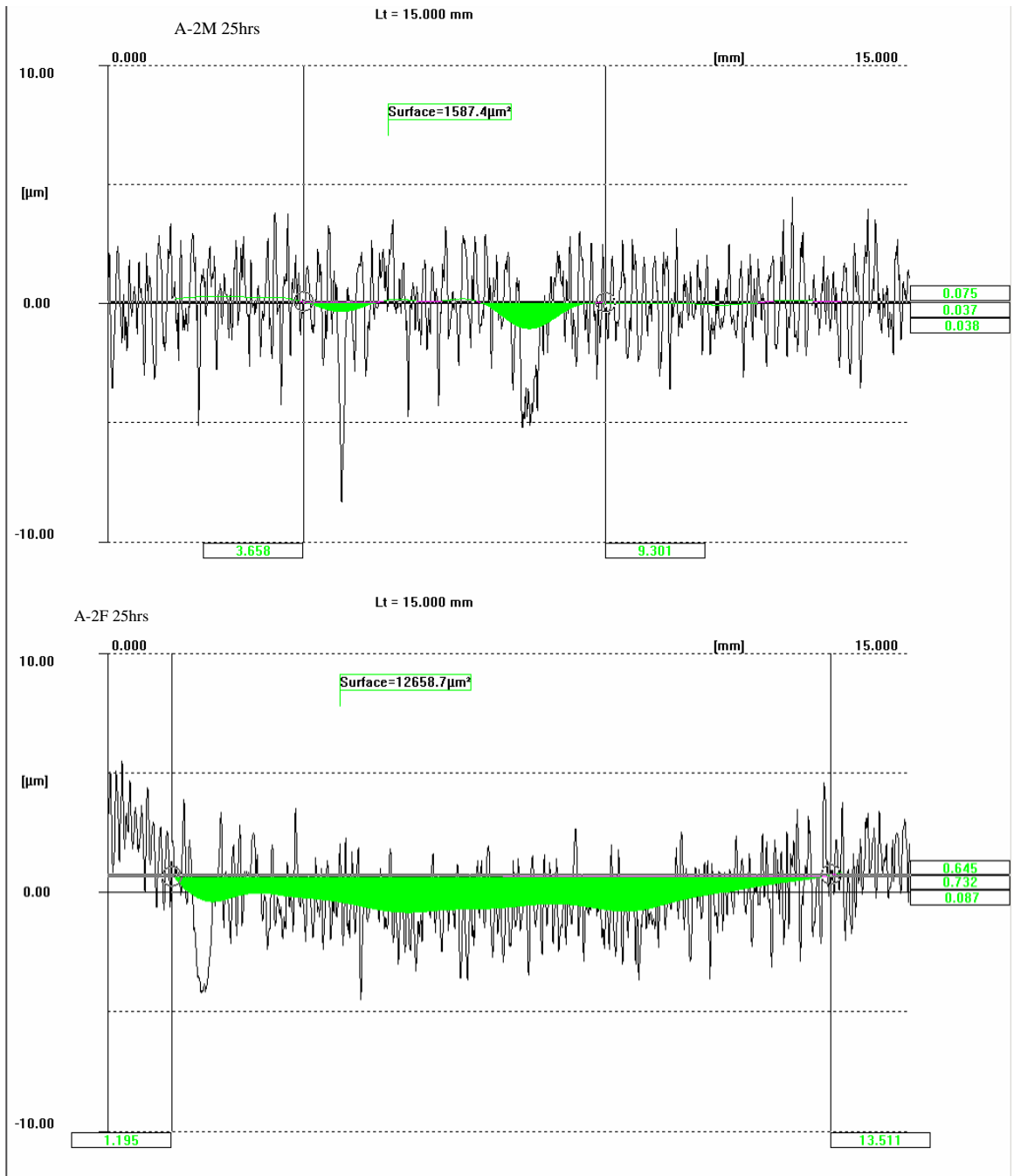
Appendix I – Wear Profiles

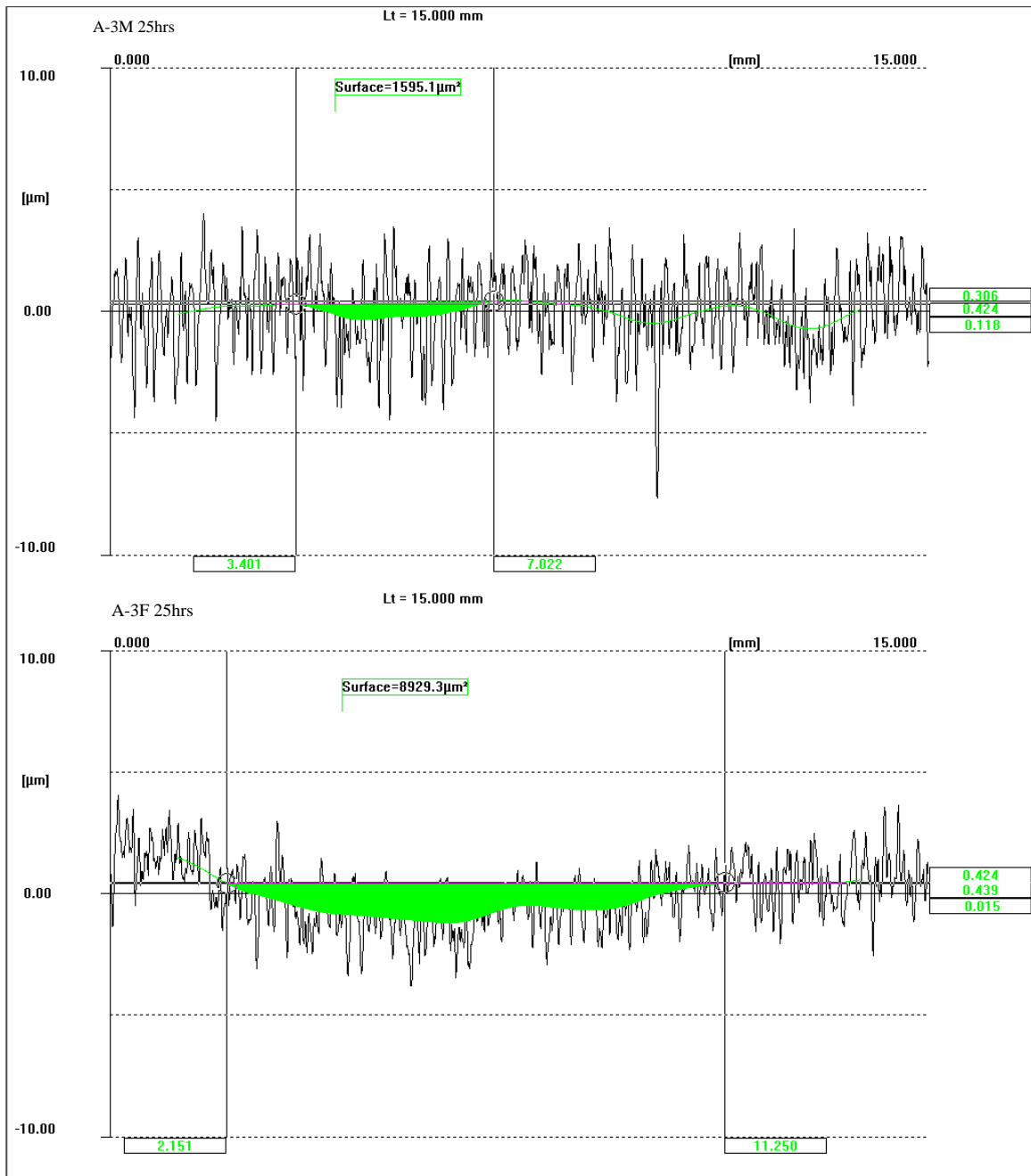


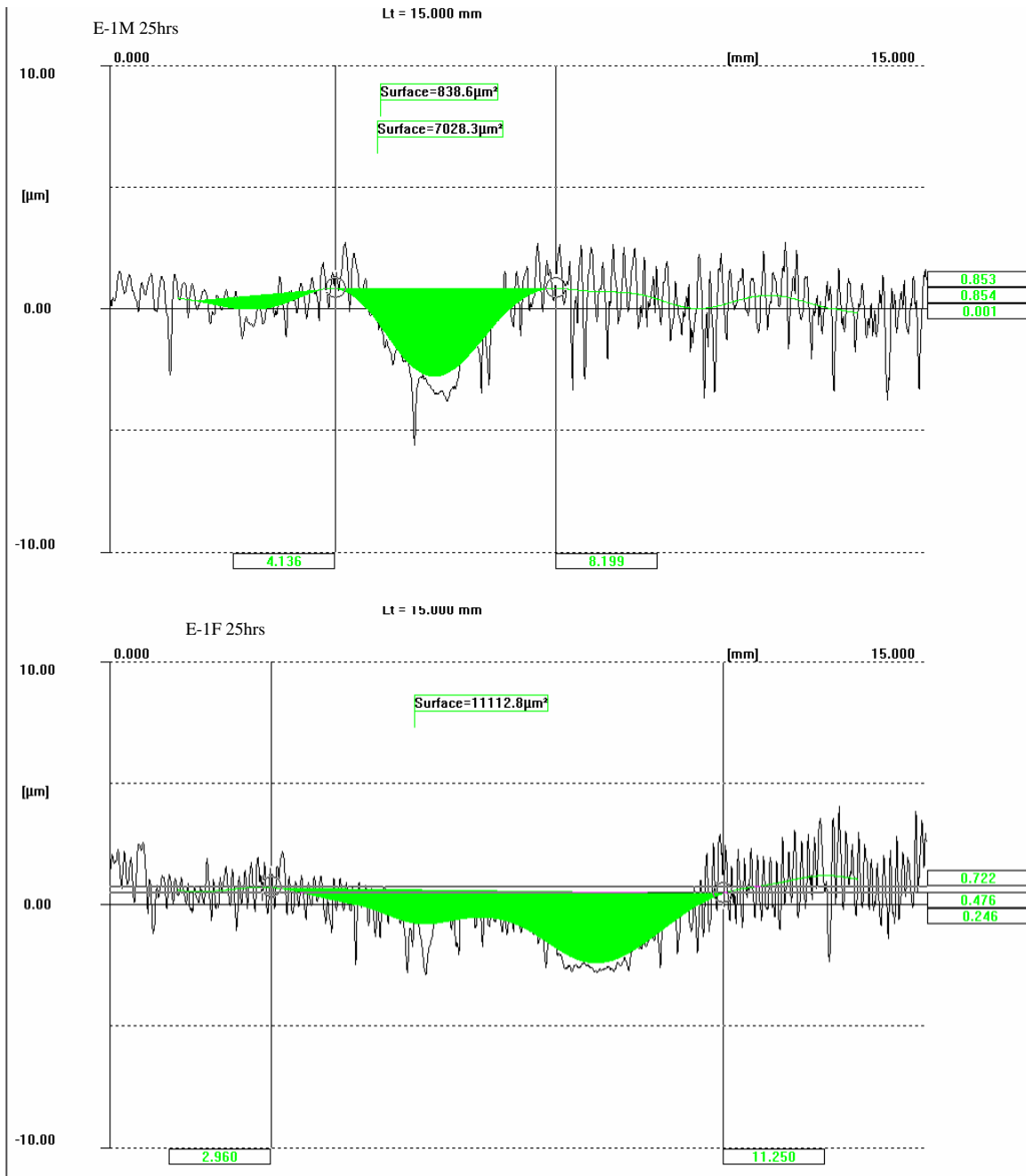


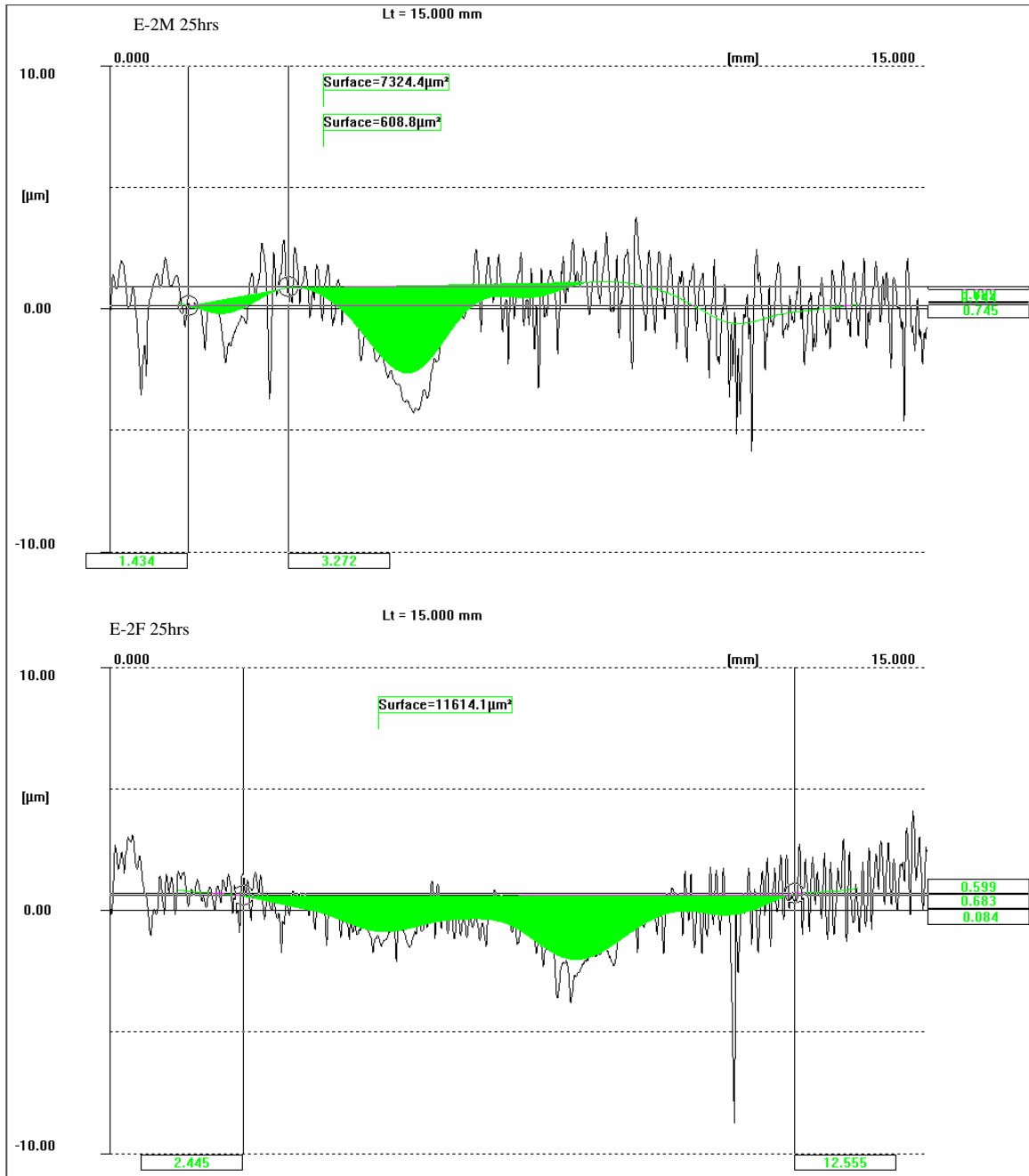


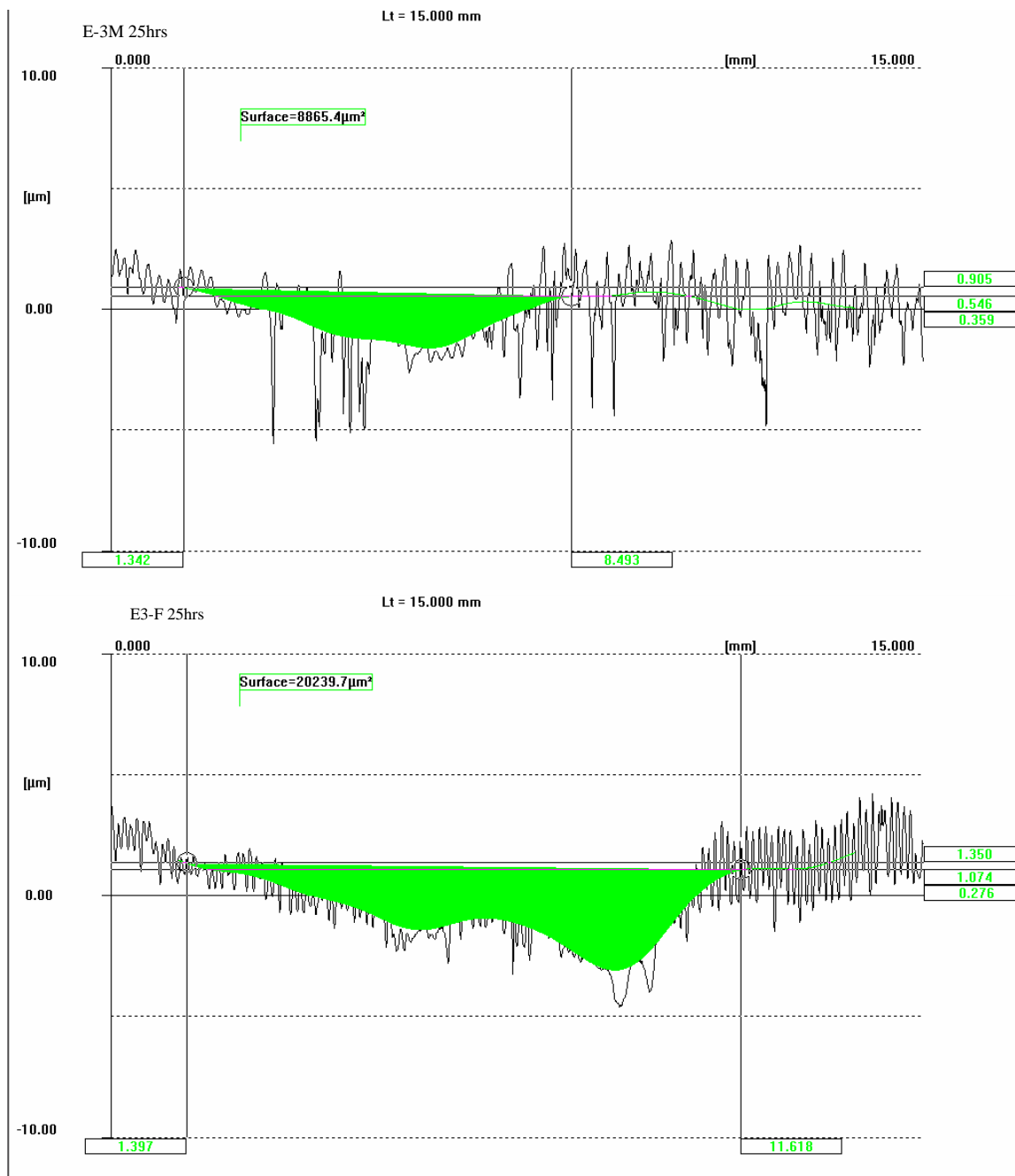


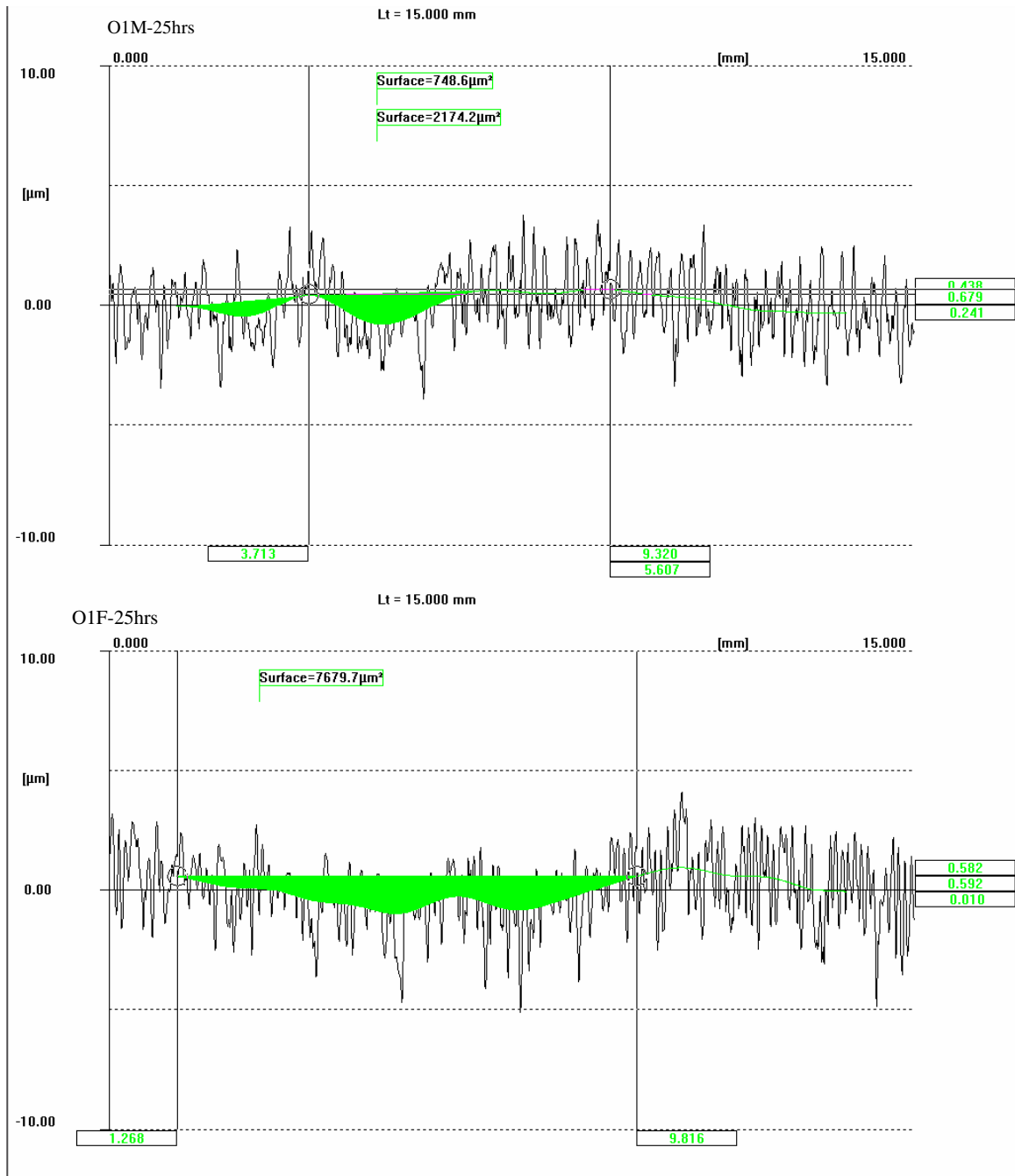












Appendix J – Plots for comparing shift delay

